Combination of pseudo-LC-NMR and HRMS/MS-based molecular networking for the rapid identification of antimicrobial metabolites from Fusarium petroliphilum

Abdulelah Alfattani, Laurence Marcourt, Valerie Hofstetter, Emerson Ferreira Queiroz, Sara Leoni, Pierre-Marie Allard, Katia Gindro, Didier Stien, Karl Perron, Jean-Luc Wolfender

Combination of pseudo-LC-NMR and HRMS/MS-based molecular networking for the rapid identification of antimicrobial metabolites from *Fusarium petroliphilum*

Abdulelah Alfattani[1,2], Laurence Marcourt[1,2], Valerie Hofstetter[3], Emerson Ferreira Queiroz[1,2], Sara Leoni[4], Pierre-Marie Allard[1,2], Katia Gindro[3], Didier Stien[5], Karl Perron[4] and Jean-Luc Wolfender[1,2*]

[1] School of Pharmaceutical Sciences, University of Geneva, 1211 Geneva 4, Switzerland

[2] Institute of Pharmaceutical Sciences of Western Switzerland, ISPSO, University of Geneva, 1211 Geneva 4, Switzerland

[3] Agroscope, Institute for Plant Production Sciences IPS, Route de Duillier 50, P.O. Box 1012, 1260 Nyon, Switzerland

[4] Microbiology Unit, Department of Botany and Plant Biology, University of Geneva, Quai Ernest-Ansermet 30, 1211 Geneva 4, Switzerland.

[5] Sorbonne Université, CNRS, Laboratoire de Biodiversité et Biotechnologie Microbienne, USR3579, Observatoire Océanologique, 66650 Banyuls-sur-mer, France.

*** Correspondence:**
Jean-Luc Wolfender
Jean-Luc.Wolfender@unige.ch

Keywords: *Posidonia oceanica*, fungal endophytes, ***Fusarium petroliphilum*, UHPLC-HRMS/MS molecular networking,** high resolution semi-preparative liquid chromatography, LC-NMR coupling, a**ntimicrobial natural products, anti-quorum sensing assays**

Abstract

An endophytic fungal strain isolated from a seagrass endemic to the Mediterranean Sea (*Posidonia oceanica*) was studied in order to identify its antimicrobial constituents and further characterize the composition of its metabolome. It was identified as *Fusarium petroliphilum* by in depth phylogenetic analyses. The ethyl acetate extract of that strain exhibited antimicrobial activities as well as an ability to inhibit quorum sensing of *Staphylococcus aureus*. To perform this study with a few tens of mg of extract, an innovative one step generic strategy was devised. On one side, the extract was analyzed by UHPLC-HRMS/MS molecular networking for dereplication. On the other side semi-preparative HPLC using a similar gradient profile was used for a single step high resolution fractionation. All fractions were systematically profiled by ^{1}H-NMR. The data were assembled into a 2D contour map, that we call "*pseudo*-LC-NMR", and combined with those of UHPLC-HRMS/MS. This further highlight connection within structurally related compounds, facilitates data interpretation and provides an unbiased quantitative profiling of the main extract constituents. This innovative strategy led to an unambiguous characterization of all major specialized metabolites of that extract and to the localization of its bioactive compounds. Altogether this approach identified 22 compounds, 13 of which being new natural products and 6 being inhibitors of the quorum sensing mechanism of *S. aureus* and *Pseudomonas aeruginosa*. Minor analogues were also identified by annotation propagation through the corresponding HRMS/MS molecular network which enable a constituent annotation of 27 additional metabolites. This approach was designed to be generic and applicable to natural extracts of the same polarity range.

1 Introduction

The rapid and efficient identification of novel natural products (NPs) in complex biological systems is a priority for the search for new lead compounds. In this context, the development of approaches that allow both rapid and unambiguous identification of natural extracts constituents as well as estimation of their biological activity are key to NP research. This is particularly true in the context of the search for antibacterial/anti-infective compounds from microorganism cultures that are often obtained on a small scale in screening programs dedicated to finding new molecules to combat the challenging resistance problems in the field (Paytubi et al., 2017).

Following a physical isolation, a classical approach for the structural determination of a metabolite naturally consists of combining high-resolution mass spectrometry (HRMS) and nuclear magnetic resonance (NMR) data to obtain a definitive identification (Yu et al., 2019). To speed up this process, HPLC coupling with NMR has proven to be an interesting alternative to work directly in mixtures, but also has some limitations. On-line and at-line LC-^{1}H-NMR hyphenations have permitted to partly characterize natural extracts metabolome (Dias and Urban, 2009; Vásquez-Ocmín et al., 2016; Hammerl et al., 2019). However, they are limited by their low sensitivity and resolution, in addition to practical issues such as solvent compatibility and solvent suppression. One way to solve these problems and to improve both spectral quality and sensitivity has been the development of LC-SPE-NMR approaches (Exarchou et al., 2005; Richard et al., 2013). Several recent works demonstrate the interest of this approach to work on natural extracts (Cardoso et al., 2016; Zebiri et al., 2016; Gad et al., 2018). A limitation, however, may be that this approach often requires repeated collection of chromatographic peaks in order to yield sufficient amounts of metabolites from given LC peaks of interest.

In this study, we developed an alternative approach to obtain consecutive NMR spectra of all fractions from a single high-resolution semi-preparative HPLC injection which is hereafter defined as *pseudo*-LC-NMR. This approach enables NMR analyses obtained at the semi-preparative level to be directly linked to UHPLC-HRMS metabolite profiling at the analytical scale with high spectral quality data on both NMR and MS dimensions. The combination of these MS, HRMS and NMR data, fraction by fraction, often allows an unambiguous identification of the metabolites present and an estimation of their amounts in parallel to biological activity tests. On the other hand, working on a semi-preparative scale enables a collection of numerous metabolites in the low mg range, a scale compatible with different types of biological tests. In this study, such an approach was applied to a fungus of marine origin (*Fusarium petroliphilum*) isolated from *Posidonia oceanica*. It allowed the identification of the metabolites responsible for antibacterial activity and obtaining a good overview of the metabolome composition of this endophytic strain.

The proposed method in this work was applied as part of a research effort to encounter new antibiotics. The emergence of resistant bacterial strains against the classical antibiotics represents indeed a major health issue (Hernando-Amado et al., 2019). New chemical entities with original activity profiles are particularly needed in drug discovery to fight such multi-resistant pathogenic bacterial strains (Brown and Wright, 2016). Among these multi-resistant bacteria, special attention must be paid to methicillin-resistant *Staphylococcus aureus* (MRSA) and *Pseudomonas aeruginosa* (PA). The gram-positive bacterium *S. aureus* causes superficial and potentially fatal infections, such as sepsis and pneumonia (Holden et al., 2013; Foster et al., 2014). The gram-negative bacterium *P. aeruginosa* is an opportunistic pathogen considered to be life-threatening to immunocompromised patients and to cystic fibrosis patients, in addition, it is a major cause of sepsis upon burn injuries (Church et al., 2006).[4] Unfortunately, currently available antibiotics are often ineffective against multi-resistant bacterial strains due to the loss of their efficacy against what are now called "superbugs" (Cordell, 2000; Foster et al., 2014). In this respect, the discovery of molecules which are capable of blocking quorum sensing (QS) could offer promising alternative to current antibiotics. Indeed, QS or cell-to-cell communication in bacteria is a regulatory process, governed by chemical signaling, that ensures sufficient cell density before inducing the expression of certain genes, at the same time throughout the bacterial population. In the case of pathogens, these genes often code for virulence factors. The disruption of this system can therefore limit the virulence of pathogenic bacteria (Bassler and Losick, 2006; Ng and Bassler, 2009; Saeki et al., 2020).

In this context, NPs and their derivatives represent a historical source of unique chemical scaffolds with potential anti-infective properties. They represent 55% of FDA-approved antibiotics introduced in the period 1981-2019 (Newman and Cragg, 2020). This underlines the importance of NPs, always valuable as a source of chemical entities for new treatments of bacterial diseases. At present, the majority of naturally originated antibiotics have been isolated from soil microorganisms. Thus, investigation of specialized metabolites from marine microbial strains in this regard is an expanding field (Blunt et al., 2018; Sun et al., 2019).

Microbial communities which often exist in competitive environments with other strains are evolving specialized metabolites pathways to produce a wide range of chemical entities which could be an interesting source of novel NPs with antibiotic activity (Peric-Concha and Long, 2003). In this relation, metabolomics study of endophytes communities is a first step to orient further drug discovery approaches on such sources. Endophytes are organisms, often fungi and bacteria that live inside plant tissues (Nisa et al., 2015). They establish different relationships with plants that vary

from symbiotic to border on pathogenic. Endophytes have shown promising potential as source of new and bioactive NPs by having evolved a diversity of specialized metabolites (Singh et al., 2017). Among the possible sources of NPs from endophytes, the marine-derived fungus *F. petroliphilum* isolated from *Posidonia oceanica* (Posidoniaceae) was chosen in this work. *P. oceanica* is an underwater sea grass endemic to the Mediterranean Sea, it forms dense meadows from the surface down to 40 m depth. *P. oceanica* is known for its longevity and being potentially the host for a diverse endophyte community. The species is endangered due to intense human activities. *P. oceanica* plays an important role at the ecological and sedimentary level (Vassallo et al., 2013).

2 Results

In order to select a bioactive fungal strain and to rapidly identify the metabolites responsible from this activity, the following procedure was applied in this study. 1) A bioactivity screen was performed on a set of *Posidonia* fungal endophytes. 2) The most active strain was prioritized for the study. 3) An aliquot from the extract was subjected to UHPLC-HRMS and automated data-dependent acquisition MS/MS for metabolite profiling followed by dereplication of known compounds through molecular network analysis. 4) Since the annotated compounds were not reported to act as QS inhibitors, their unambiguous characterization had to be performed. 5) In order to localize and identify the bioactive compounds, the fungal extract was thoroughly analyzed by *pseudo*-LC-NMR (Figure 1F). The *pseudo*-LC-NMR process was developed for the purpose of this study but was intended to be generic in order to rapidly provide complementary NMR information to the LC-MS metabolite profiling of crude extracts available in limited amounts.

The key steps for this approach were as follow: 1) An optimized geometrical transfer was applied from the scale of UHPLC to analytical HPLC then to semi-preparative HPLC (Figure 1A, D and E). 2) The crude extract was injected by LC at the semi-preparative scale with automated fraction collection each 30 seconds. 3) All fractions were submitted to ^{1}H-NMR analyses followed by LC-HRMS/MS. 4) ^{1}H-NMR spectra were stacked and plotted in 2D map sequenced according to retention time generating the *pseudo*-LC-NMR plot. 5) The concomitant processing of the *pseudo*-LC-NMR with the LC-MS profile allowed to increase the level of annotation and to conduct specific 2D-NMR experiments when needed.

In order to localize the bioactivity, the fractionation strategy had to be adapted to the sensitivity of the assays. In this specific study, the measurement of antibacterial and anti-QS activity required larger quantities than those obtained from the 30 seconds/fraction at the semi-preparative scale described above. Thus, a pooling of fractions was designed to highlight the area of chromatographic activity (Figure 1D,E). This finally permitted conducting a specific targeted purification of bioactive compounds on enriched extract with the same experimental setting.

2.1 Identification of the fungal strains

The identification of the marine strain *F. petroliphilum* that is the subject of this study proved to be challenging as this species is part of a species complex of *Fusarium solani*. Its identification required its placement within this complex in which terrestrial species are also found.

Although ITS is presently the best barcode sequence for fungi (Schoch et al., 2012), it did not allow the assignment of the selected fungal strain, FEP 16, at species rank. BLAST top score results in GenBank (GB) indicated that the FEP 16 ITS sequence was 100% similar with a 100% coverage, to the sequences of several species: *F. petroliphilum* (Q.T. Chen & X.H. Fu) D. Geiser, O'Donnell,

Short & Zhang 2013 (GB accession number: LC512834), *F. macroceras* Wollenweber & Reinking 1925 (MH854821) and *F. solani* Mart. 1842 (MH855493). These species, based on ITS BLAST results, belong to the *F. solani* species complex in which many species are still not formally described (Short et al., 2013; Chehri et al., 2015; O'Donnell, 2019). Trying to determine further to which species FEP 16 belongs, we sequenced four more loci for that strain (see experimental section) and combined these data with data sampled in Bohni et al. (2016). Unfortunately for *F. macroceras*, only ITS and part of the nuclear large subunit (28S) were available in GB. After similarity search of the 28S (MH866321) of *F. macroceras* in GB, that sequence appeared 100% similar with several sequences for *F. solani* (i.e. AY097317) with 100% of sequence coverage but also with four sequences for *F. petroliphilum* (i.e. MH874378) but with 90% of sequence coverage. Consequently, these two taxa are likely to be identical but without sequences for other more variable loci (*RPB2*, beta-tubulin and calmodulin) for *F. macroceras* but it is not possible to clarify the situation without type sequences for these species. Combined analyses for the *Fusarium* 5 locus-81 taxa (Figure 2) (Supplementary Table S1) allowed to identify FEP 16 as *F. petroliphilum*.

2.2 Evaluation of the antibacterial activity of the crude extracts

The minimum inhibitory concentration (MIC) of the extracts of all strains were tested against a methicillin-resistant strain of *Staphylococcus aureus* (ATCC 33591-MRSA) and a strain of *Pseudomonas aeruginosa* (ATCC 27853) (Supplementary Table S2). The crude extract of the fungus *F. petroliphilum* (FEP 16) presented an antibacterial activity against MRSA with a MIC at 32 µg/mL but no activity against Gram-negative *P. aeruginosa* strain.

In order to further verify if activity could be revealed at the level of quorum sensing (QS) inhibition for *P. aeruginosa*, we performed a reporter assay based on percentage of fluorescence to evaluate the potential of the crude extract on QS (Hentzer et al., 2002). Interestingly, the crude extract displayed about 80% reduction of the fluorescence level of 2 reporter genes (*pqsA* and *lasB*) normally induced by QS in *P. aeruginosa* (Table 1). The *pqsA* gene encodes an enzyme involved in the synthesis of PQS which is a signaling molecule of QS, while the *lasB* gene encodes an important elastase enzyme (Jimenez et al., 2012). These primary bioassay results encouraged us to go for further investigations.

2.3 Metabolites dereplication by UHPLC-HRMS/MS

In order to have a primary overview of the crude extract chemical content, it was analyzed by UHPLC-HRMS/MS in positive (PI) and negative (NI) ionization modes, MS/MS spectra of all detected features were recorded by data dependent analysis (DDA). Feature-based molecular networks (Nothias et al., 2020) for both modes were built to arrange the extracted ions (precursor ions) into clusters based on MS/MS similarity. This process was done by filtering ions below an intensity threshold at 1E6 and yielded 1900 features in PI mode, and 2270 in NI mode for building the corresponding MNs (Supplementary Figures S1,S2). The precursor masses and their associated MS/MS spectra were matched against experimental data from GNPS as well as predicted spectra obtained by *in silico* MS/MS fragmentation database (ISDB-DNP) (Allard et al., 2016).

For each node of the MN, possible structure candidates were listed according to MS/MS similarity (initial rank) up to a maximum of top 50 compounds reported to occur in fungi. To increase the level of confidence in annotation, a reweighting step based on taxonomy was performed. This step takes into consideration the matching between the biological source reported in the DNP at level of species > genus > family, resulting in a maximum of top 5 candidate compounds (final rank) for

each annotated node (Rutz et al., 2019). As a result, in PI mode, 823 of the 1900 detected features were annotated, 214 of them were found in family Nectriaceae, 148 of them present in genus *Fusarium* and 28 features reported in closely related species *F. solani*. In NI mode, 705 features were annotated out of 2720, 200 of them belonging to Nectriaceae, 135 of them were reported in the same genus and 19 of them have been found in *F. solani*. The annotated metabolites corresponding to the most intense MS peaks detected in both PI (threshold > 5E7) and NI (threshold > 1E7) are presented in Table 2. Their annotation was further refined by taxonomical ranking and by structural consistency of corresponding clusters. Compounds not previously found at least in the Nectriaceae family were not considered in this LC-MS dereplication process. The full MNs with the complete annotation is deposited in Figshare (https://doi.org/10.6084/m9.figshare.14706198). The same MN will be used later on this study to apply annotation propagation through location of isolated molecules in the MN.

Most of the annotated metabolites belong to pyran and pyrone derivatives, furan lactones, naphthoquinones, isocoumarins, terpenes and sterols. Such data are consistent with previously reported studies on the chemical content of *Fusarium* species (Wei and Wu, 2020). In particular, the presence of some frequently reported compounds in *Fusarium*, such as, gibepyrone D (Wang et al., 2011), aloesol (Kashiwada et al., 1984), fusarubin (Tatum and Baker, 1983), anhydrofusarubin (Shao et al., 2010) and bostrycoidin (Arsenault, 1965) which were highlighted in Table 2. As shown in Table 2, more than 30% of the most intense MS peaks could not be annotated through this process which could be either unknown compounds or compounds never reported in the Nectriaceae family.

Based on these dereplication results and the bioactivity data measured on the extract, this prompted us to establish an efficient approach that should provide complementary NMR data in line with metabolite profiling. This workflow is designed to run with few tens of milligrams of active extract, which corresponds to the usual amount obtained at laboratory scale using conventional Petri dishes (about 100 plates).

2.4 Culture scale-up and semi-preparative HPLC fractionation

In order to obtain enough material to continue our proposed workflow, the culture of *F. petroliphilum* was scaled up to 100 petri dishes under the conditions described in materials and methods. This yielded 300 mg of ethyl acetate crude extract which exhibited bioactivity results comparable to those obtained during screening (Table 1).

To effectively link the expected fractionation of this extract with the metabolite profiling data (see above), a chromatographic gradient transfer method was used to find the correct separation parameters, ideally for a single separation at the semi-preparative level. In practice, an intermediate step at the analytical HPLC level (Figure 1D) was necessary on a column having the exact same phase chemistry as the one used in the semi-preparative level (see experimental section). The optimum HPLC conditions were determined with UV monitoring at 254 nm. This latter linear gradient method was then geometrically transferred to the semi-preparative scale. (Guillarme et al., 2008)

In order to obtain an efficient high-resolution separation of this complex mixture and to avoid any loss of chromatographic resolution, the crude extract (40 mg) was introduced into a dry loading cell according to our previously published protocol (Queiroz et al., 2019). Using this approach, it was possible to obtain equivalent separations at analytical and semi-preparative scales (Figure 1A, D

and E). To match the high chromatographic resolution that was obtained, 135 fractions were automatically collected on the basis of one fraction per 30 seconds. All fractions were immediately dried under vacuum and weighted.

2.5 Combination of NMR spectra for an overview as a *pseudo*-LC-NMR plot

With the idea to obtain a comprehensive NMR profile of all fractions and be able to align all spectra over the extended polarity range of the various metabolites separated, each fraction was diluted in 600 µL of DMSO-d_6 and submitted to ^{1}H-NMR analysis. DMSO-d_6 was selected since it is known to have good solubility properties and for its compatibility with bioassays. The ^{1}H-NMR spectra of all fractions were obtained by automated acquisition (29 hours of total acquisition). In order to visualize all ^{1}H-NMR signals from the 135 fractions (F1-F135), a 2D plot was generated. For this, all individual spectra were binned and combined into a single matrix (ppm vs. RT or fraction Nº). This plot simulates the actual output of a classic on-flow LC-NMR analysis (Queiroz et al., 2002). The chromatographic dimension of the plot was expressed either as fraction number or retention time since all spectra were stacked according to their elution order, which allows a straightforward correlation with the corresponding analytical HPLC-PDA trace (Figure 1F). An interactive version of the plot can be explored here: (https://oolonek.github.io/pseudo_lcnmr_plotter/2dNMR.html).

The generated 2D plot from collected and dried micro-fractions has several advantages over classical LC-NMR. In this case, all ^{1}H-NMR signals are perfectly aligned, since all spectra are recorded with the same solvent across the whole separation (DMSO-d_6). By comparing our approach to on-flow LC-NMR, no solvent suppression is necessary. In addition, compared to at-line LC-NMR detection methods, such as LC-SPE-NMR (Chang et al., 2020), the spectra obtained are recorded from a single LC separation and multiple injections for sample enrichment are not necessary. We define this workflow as a *pseudo*-LC-NMR analysis which can be viewed either as a 2D plot (Figure 1F) or as a stacked view (Figure 3A) for a comprehensive analysis of the evolution of the ^{1}H signals across the chromatographic dimension. Since the NMR response is directly proportional to the amounts of compounds, the overall observation of the 2D plot provides in a first instance an unbiased view of the molar ratios between constituents. However, this of course also related to the number of magnetically diverse protons for each constituent.

In order to determine molar ratios between fractions, a histogram was created based on ^{1}H-NMR peak integration which represents total proton intensities of each recorded spectrum (Supplementary Figure S3A). This histogram was rather similar to the one obtained by weighed dry fractions (Supplementary Figure S3B) which shows mainly major apolar constituents eluting at the end of the chromatogram between fractions F110 and F132. Analysis of the related ^{1}H-NMR spectra revealed signal patterns which mainly correspond to fatty acids, i.e., a methyl group at δ_H 0.5 and an intense signal from methylene protons around δ_H 1.25. A specific histogram based on the methylene chain signal found typically in fatty acids was built across all fractions, it allows to highlight their presence mainly in fractions F110, 111, 114, 115, 117, 118, 119, 122 and 123 (Supplementary Figure S3C). This trace matches well with the ELSD detection as shown in Supplementary Figure S3D and demonstrates that the crude extract was dominated by apolar constituents. Most of these fatty acids were found to be unsaturated fatty acids and exhibited a characteristic signal of their ethylenic protons around δ_H 5.3 whereas fractions F117, 122 and 123 contain saturated fatty acids.

In addition to fatty acids, steroids and triterpenes were also identified in this chromatographic region. For example, ergosterol (**22**) a main constituent of fungal membrane, could be identified in F132 yielding an intense signal in the histogram (Supplementary Figure S3A). Its ^{1}H-NMR spectrum was in good agreement with reported data (Kwon et al., 2002; Yang et al., 2003) and confirming the dereplication results (Table 2). Moreover cerevisterol (**20**), could be confirmed in F116 by comparing its ^{1}H-NMR spectrum with literature (Kawagishi et al., 1988). Based on the extraction procedure, the presence of these main common apolar fungal constituents is not surprising. The analysis of the *pseudo*-LC-NMR 2D plot facilitated their identification and estimations of the ratio in an unbiased manner.

Further inspection of this *pseudo*-LC-NMR plot revealed the presence of specialized metabolites with aromatic signals (between δ_H 6.5 and 8.0) which were easily identified at the beginning of the chromatogram (F1-27). In this part of the semi-preparative HPLC chromatogram, the LC-UV profile exhibited main peaks that were mostly not fully separated (Figure 1E). The inspection of the 2D plot as well as the related ^{1}H-NMR profile of each fraction was in line with this observation and exhibited spectra with overlapping signals. In this polar region, several compounds dereplicated by HRMS/MS (Table 2) could be confirmed by NMR upon comparison with reported data of the literature: adenosine (**1**) (Ciuffreda et al., 2007) was identified in fraction F4, gibepyrone D (**4**) (Wang et al., 2011) in fraction F20, aloesol (**5**) (Kashiwada et al., 1984) in fraction F26. In this region of the chromatogram arthropsolide A (Ayer et al., 1992) (Table 2) was dereplicated by HRMS/MS but in this case it could not be confirmed by ^{1}H-NMR, this could indicate that this common *Fusarium* metabolite is most likely present but in quantities below the NMR detection limit.

In the intermediate region of the chromatogram (fractions F28-F109), three known compounds which are common to *Fusarium* were dereplicated by HRMS/MS, bostrycoidin (**11**) (Arsenault, 1965), fusarubin (**7**) and 3-*O*-methylfusarubin (**8**) (Tatum and Baker, 1983) which were confirmed by ^{1}H-NMR in F60 for **11** and in mixture in F43 and F44 for **7** and **8** respectively. Gibepyrone A (Westphal 2018) was dereplicated by HRMS/MS and confirmed by some of its characteristic ^{1}H-NMR signals in fraction F42, this compound was however present in very low concentration. In addition, minor metabolites dihydroanhydrojavanicin (Tatum et al., 1989) and solaniol (Niu et al., 2019) were dereplicated by HRMS/MS only but could not be found in NMR (Table 2). In this medium polarity region, several fractions (F51-56 and F91-93) seem to have ^{1}H signals in common particularly in the regions between δ_H 5.5 and 5.7, and between δ_H 6.0 and 6.3 (Figure 3A, highlighted in green), indicating that these fractions may contain structures with close skeletons (**9**, **10**, **16**, and **17**). Another class of molecules (cyclohexanones) could be highlighted in fractions F64-65 and F103-104 which were characterized by their signals between δ_H 5.2 and 5.3 (orange). The analysis of NMR spectra of these fractions, for which no confident HR-MS/MS annotation were obtained, revealed 3 new compounds (**13**, **14**, and **18**), Figure 4.

Since all NMR spectra were recorded in DMSO-d_6 the low field region (δ_H 11.0 -14.0) of the pseudo-LCNMR 2D plot highlighted characteristic deshielded mobile protons. Among them the acidic protons of fatty acids were clearly seen (δ_H 12.0) in F113-119 and quinonic phenolic groups of fusarubin (**7**) and 3-*O*-methylfusarubin (**8**) were observed (Figure 1F). Several similar types of signals were linked to the unknow metabolites in F35 and F69.

These selected examples show a good complementarity of NMR and HRMS/MS data for the dereplication of main constituents and help highlighting new *Fusarium* metabolites. For full *de*

novo structure identification 2D-NMR spectra were recorded for the compounds of interest and those exhibiting sufficient S/N ratio in the ^{1}H-NMR spectra.

2.6 Structure elucidation of new compounds

Careful interpretation of the HRMS/MS and ^{1}H-NMR data resulted in the identification of twenty-two compounds in one-step (**1**-**22**), among them, 13 are original NPs described here for the first time (**2a**/**2b**, **3**, **6**, **9**, **10**, **12**, **13**, **14**, **15**, **16**, **17**, **18**, **19**) and presented in Figure 5. The known dereplicated compounds described above were also confirmed, when necessary, by additional 2D-NMR data and were all previously reported in *Fusarium* species: adenosine (**1**) (Hou et al., 2015), gibepyrone D (**4**) (Wang et al., 2011), aloesol (**5**) (Kashiwada et al., 1984), fusarubin (**7**) and 3-*O*-Methylfusarubin (**8**) (Tatum and Baker, 1983), bostrycoidin (**11**) (Yamamoto et al., 2002), cerevisterol (**20**) (Wang et al., 2011), 6-Dehydrocerevisterol (**21**) (Qiao et al., 2017) and ergosterol (**22**) (Thammawong et al., 2011).

Compound **6** (F35) was isolated as a pale rose amorphous solid. The HRMS/MS spectrum showed a molecular ion at *m/z* 288.0846 $[M + H]^{+}$ (calculated for $C_{15}H_{14}NO_5$, 288.0866). No valid annotations based on MS could be obtained for this compound among all Nectriaceae described metabolites. The ^{1}H and edited-HSQC NMR spectra showed 3 exchangeable protons at δ_H 5.06 (1H, t, *J*=5.6 Hz, OH-15), 11.39 (1H, s, NH-13) and 12.88 (1H, s, OH-5), two aromatic protons at δ_H 6.23 (1H, s, H-3) and 6.44 (1H, dd, *J*=2.1, 1.1 Hz, H-11), an oxymethylene at δ_H 4.75 (2H, d, *J*=5.5 Hz, H_2-15) and a methoxy group at δ_H 3.89 (3H, s, H_3-16) and a methyl at δ_H 2.44 (3H, d, *J*=1.0 Hz, H_3-14). A methoxy naphthoquinone moiety such as that found in fusarubin (**7**) was identified, thanks to the HMBC correlations from H-3 to the carbonyl C-4 (δ_C 191.0) and C-1 (δ_C 179.5) to the quaternary carbons C-2 (δ_C 160.5) and C-10 (δ_C 107.4), and from the methoxy group to C-2. The methoxy signals were clearly shared in the *pseudo*-LC-NMR plot between compound **6** (F35) and the two furarubins **7** and **8** (F43-F44) this was also clearly visible for the common H-3 aromatic signal of these molecules (Figure 4). The HMBC correlations from the deshielded hydroxyl OH-5 to C-10, C-5 (δ_C 152.1) and C-6 (δ_C 126.8) and from the oxymethylene H_2-15 to C-5, C-6 and C-7 allowed to position these two groups. Then, a 2-methyl-pyrrole group was placed in C7-C8 according to the HMBC correlations from the aromatic proton H-11 to C-6, C-7 and C-8 (δ_C 130.5), from the methyl protons H_3-14 to C-11 (δ_C 99.8) and C-12 (δ_C 156.7) and from NH-13 to C-7, C-8, C-11 and C-12. The ROESY correlations from H-3 to the methoxy H_3-16 and from H-11 to H_2-15 and H_3-14 confirmed the structure. Compound **6** was thus identified as 5-hydroxy-4-(hydroxymethyl)-8-methoxy-2-methyl-1H-benzo[g]indole-6,9-dione.

The HRMS/MS spectrum of **9** (F51) displayed a molecular ion at *m/z* 295.1542 $[M + H]^{+}$ corresponding to the molecular formula $C_{16}H_{22}O_5$ The NMR spectra showed 3 aromatic protons at δ_H 5.52 (1H, d, *J*=1.8 Hz, H-3), 6.11 (1H, d, *J*=1.8 Hz, H-5) and 6.15 (1H, dd, *J*=9.8, 1.4 Hz, H-8), 2 methylenes at δ_H 1.21 (1H, dt, *J*=13.4, 7.4 Hz, H-10''), 1.34 (1H, dt, *J*=13.4, 6.8 Hz, H-10'), 1.96 (1H, dd, *J*=15.0, 8.5 Hz, H-12'') and 2.25 (1H, m, H-12'), a methine at δ_H 1.79 (1H, dqd, *J*=8.5, 6.8, 5.1 Hz, H-11), 3 methyl groups at δ_H 0.89 (3H, d, *J*=6.6 Hz, H_3-14), 0.96 (3H, d, *J*=6.6 Hz, H_3-15) and 1.86 (3H, d, *J*=1.4 Hz, H_3-16) and a methoxy signal at δ_H 3.88 (3H, s, H_3-17). A 4-methoxy-6-substituted-α-pyrone was identified from the HMBC correlations between H-5 and C-3 (δ_C 88.7), C-6 (δ_C 159.6) and C-7 (δ_C 127.3), between H-3 and C-5 (δ_C 108.7), C-4 (δ_C 167.2) and C-2 (δ_C 180.2), and between H_3-17 and C-4. An alkyl side chain was attached in C-7, the HMBC correlations from H_3-16 to C-6, C-7 and C-8 (δ_C 140.0), from H_3-15 to C-8, C-9 (δ_C 29.9) and C-10 (δ_C 43.3), from H_3-14 to C-10, C-11 (δ_C 27.6) and C-12 (δ_C 40.9), and from H_2-12 to C13 (δ_C 173.7)

allowed to unambiguously assigned this 3,5,7-trimethylhept-6-enoic acid side chain. The *E* configuration of the double bond of the side chain was deduced from the ROE correlation between H_3-16 and H-9. As discussed previously on the *pseudo*-LC-NMR plot some of the ^{1}H-NMR signals of **9** were common to other metabolites (**10**, **16** and **17**) found in F55, F91 and F93 suggesting a common pyrone moiety (Figure 4). Compound **9** was identified as (6E)-7-(4-methoxy-6-oxo-6H-pyran-2-yl)-3,5-dimethyloct-6-enoic acid.

The NMR data of **10** (F55) exhibited indeed close similarities to those of **9**, they share the same 4-methoxy-α-pyrone and the difference lies in the side chain. One of the methyl doublet signals present in **9** was replaced in **10** by a methyl triplet at δ_H 0.81 (3H, t, *J*=7.3 Hz, H_3-13). An additional oxymethylene was observed at δ_H 3.25 (1H, dt, *J*=10.2, 5.0 Hz, H-14") and 3.30 (1H, dt, *J*=10.2, 5.0 Hz, H-14') in addition to a hydroxyl at δ_H 4.34 (1H, t, *J*=5.2 Hz, OH-14) whereas the carbonyl of the acid group was no longer observed. The 2D-NMR experiments were in good agreement with the structure presented in Figure 4 and the ion at *m/z* 281.1744 $[M + H]^+$ confirmed the structure as 6-((*E*)-6-ethyl-7-hydroxy-4-methylhept-2-en-2-yl)-4-methoxy-2H-pyran-2-one.

Compound **16** which has MF of $C_{16}H_{24}O_3$ and ionized at *m/z* 265.1816 $[M + H]^+$ in F91 shares the same skeleton as **9** and **10**. The carboxyl group presented at the end of the side chain of **9** was replaced in this case by a methyl group at δ_H 0.82 (3H, t, *J*=7.4 Hz, H_3-13). Compound **16** was thus identified as 4-methoxy-6-((*E*)-4,6-dimethyloct-2-en-2-yl)-2H-pyran-2-one.

Compound **17** which has MF of $C_{17}H_{26}O_3$ and ionized at *m/z* 279.1956 $[M + H]^+$ in F93 belongs also to the same family. The side chain was the same as that of **16** but an additional methyl group was observed in C-3 at δ_H 1.69 (3H, s, H_3-18). The HMBC correlations from the methyl H_3-18 to the ester carbon C-2 (δ_C 179.7), the olefinic carbon C-3 (δ_C 98.9) and the oxygenated olefinic carbon C-4 (δ_C 162.0) confirmed this structure as 4-methoxy-3-methyl-6-((E)-4,6-dimethyloct-2-en-2-yl)-2H-pyran-2-one. A zoom in the stacked plot also clearly highlights this similarity on the side chain (Figure 3D).

Compound **12** in F62 was found to possess a molecular formula of $C_{28}H_{40}O_6$ with 8 degrees of unsaturation, as evidenced by PI HRMS/MS at *m/z* 473.2877 (calcd for $C_{28}H_{41}O_6$). The ^{1}H-NMR data of **12** showed typical signals of an oxygenated steroid: 2 methyl singlets at δ_H 0.77 (3H, s, H_3-18) and 0.89 (3H, s, H_3-19), 3 methyl doublets at δ_H 0.85 (3H, d, *J*=7.0 Hz, H_3-28), 0.90 (3H, d, *J*=6.8 Hz, H_3-26) and 1.73 (3H, d, *J*=1.2 Hz, H_3-21), 4 oxygenated methines at δ_H 3.27 (1H, d, *J*=3.7 Hz, H-6), 3.59 (1H, tq, *J*=10.6, 5.0 Hz, H-3), 4.18 (1H, t, *J*=8.5 Hz, H-23) and 5.53 (1H, dd, *J*=5.2, 3.7 Hz, H-7), an oxygenated methylene at δ_H 3.31 (1H, overlapped, H-27") and 3.93 (1H, dd, *J*=8.2, 6.4 Hz, H-27'), an ethylenic proton at δ_H 5.22 (1H, d, *J*=8.4 Hz, H-22) and a series of methines and methylenes between δ_H1.20 and 2.63. The HMBC also indicated the presence of two oxygenated quaternary carbon at δ_C 68.1 (C-5) and 74.8 (C-9), two quaternary sp^2 carbons at δ_C 134.1 (C-20) and 142.8 (C-14), and a carbonyl at δ_C 206.7 (C-15). HMBC correlations from H_3-19 to C-1 (δ_C 25.6), C-5, C-9 and C-10 (δ_C 37.0), from H_3-18 to C-12 (δ_C 32.1), C-13 (δ_C 43.1), C-14 and C-17 (δ_C 51.5), from the methylene H_2-16 at δ_H 2.16 (1H, dd, *J*=18.3, 7.3 Hz, H-16α) and 2.63 (1H, m, H-16β) to C-15 allowed to identify the four member rings of sterol in compound **12** which was identical to 5β,6β-epoxy-3β,7α,9α-trihydroxy-(22E,24R)ergosta-8(14),22-dien-15-one previously isolated by Wang et al. (2012) from the culture of the Basidiomycete *Polyporus ellisii*. The chain attached to C-17 was found to be new, its linkage was established by the HMBC correlations from the methyl H_3-21 to C-17 (δ_C 51.5), C-20 and C-22 (δ_C 128.1) and thus the presence of a double bond between C-20 and C-22. The HMBC correlations from H_3-28 to C-23 (δ_C

79.7), C-24 (δ_C 42.9) and C-25 (δ_C 35.9), from H_3-26 to C-24, C-25 and C-27 (δ_C 73.7) and from H_2-27 to C-23 indicated the formation of a furan ring. The ROESY correlations from H_3-18 to H_3-21 and H-11β, from H_3-19 to H-11β and H-2β, from H-4α to H-3 and H-6, from OH-7 to H-6, from H-1α to OH-9, from H-23 to H_3-21and H_3-28, and from H-22 to H-17 and H-24 allowed to determine the relative configuration of this new sterol (Figure 5). Compound (**12**) was characterized as 5β,6β-23,26-diepoxy-3β,7α,9α-trihydroxy-(20Z,23S,24S,25R) ergosta-8(14),20-dien-15-one.

As discussed above, compounds **13**, **14**, and **18** sharing many common ^{1}H-NMR signals in the *pseudo*-LC-NMR plot were assigned to the same structural type. Among them, **18** exhibited the most intense signals and were analyzed in depth first.

Compound **18** in F103 was isolated as a pale yellow amorphous solid. The HRMS/MS spectrum showed a protonated ion at *m/z* 333.2441 corresponding to a molecular formula of $C_{21}H_{32}O_3$. The ^{1}H and HSQC NMR spectra displayed two ethylenic protons at δ_H 5.25 (1H, dd, *J*=15.2, 7.9 Hz, H-15) and 5.29 (1H, dd, *J*=15.2, 7.0 Hz, H-16), five methylenes at δ_C 27.2 (C-16), 27.3 (C-15), 30.9 (C-7), 32.7 (C-11), 35.8 (C-12), four methine at δ_C 32.4 (C-25), 38.1 (C-20), 42.0 (C-24), 55.4 (C-17), four methyl doublets at δ_H 0.81 (3H, d, *J*=6.9 Hz, H_3-27), 0.83 (3H, d, *J*=6.9 Hz, H_3-26), 0.91 (3H, d, *J*=6.7 Hz, H_3-28), 1.03 (3H, d, *J*=6.6 Hz, H_3-21) and one methyl singlet at δ_H 1.06 (3H, s, H_3-18). The HMBC correlations from methyl H_3-18 to the methylene C-12, the quaternary carbon C13 (δ_C 44.6), the sp^2 carbon C-14 (175.2) and the methine C-17, from the methylene H_2-7 to C-14, the sp^2 carbon C-8 (δ_C 125.0), the carbonyl C-9 (δ_C 196.3) and to the carboxyl C-6 (δ_C 171.7), from the methylene H_2-11 (δ_H 2.22 and 2.56) to C-6 and H_2-15 (δ_H 2.34 and 2.46) to C-14 and C-17 in combination with COSY correlation from H_2-11 to H_2-12 (δ_H 1.79 and 2.15) and H-17 (δ_H 1.42) to H_2-16 (δ_H 1.51 and 1.78) allowed to identify a fused six- and five-membered rings. The side chain in C-17 was identified and positioned thanks to the HMBC correlation from the methyl H_3-21 to the methines C-17 and C-20 and the olefinic carbon C-22 (δ_C 134.7), from the methyl H_3-28 to the olefinic carbon C-23 (δ_C 132.0), the methines C-24 and C-25 and from the methyls H_3-26 and H_3-27 to the methines C-24 and C-25. This compound corresponds to a highly degraded ergostane-type steroid identified as 2-(2,3,5,6,7,7a-hexahydro-7a-methyl-1-((*E*)-5,6-dimethylhept-3-en-2-yl)-5-oxo-1H-inden-4-yl)acetic acid.

The NMR signals of the isomeric **13** and **14,** both possess MF of $C_{21}H_{32}O_4$ and protonated ions at *m/z* 349.2349, showed great similarities with those of **18** in F103 ($C_{21}H_{32}O_3$), except for the terminal part of the side chain. Compound **13** contains an additional hydroxy group in C-25 evidenced by the HMBC correlations from the methyls H_3-26 and H_3-27 (δ_H 1.03 and 0.99, respectively) to the oxygenated quaternary carbon C-25 (δ_C 70.5) and the methine C-24 (δ_C 47.1). In compound **14**, the terminal methyl H_3-27 was hydroxylated and replaced by an oxygenated methylene at δ_H/δ_C 3.17/64.4.

Compound **15** (F69) was found to possess a molecular formula of $C_{14}H_{13}NO_4$ and showed a deprotonated ion at *m/z* at 258.0771 $[M - H]^-$. It was isolated as a pale yellow amorphous solid, its ^{1}H and HSQC NMR spectra indicated the presence of two mobile protons at δ_H 11.39 (1H, s, NH-11) and 12.84 (1H, s, OH-6), two aromatic protons at δ_H 6.21 (1H, s, H-3) and 6.28 (1H, s, H-9), one methoxy group at δ_H 3.89 (3H, s, H_3-14) and two methyl groups at δ_H 2.36 (3H, s, H_3-15), 2.44 (3H, s, H_3-16). The HMBC correlation from the methyl H_3-16 to only two olefinic carbons C-9 and C-10 at δ_C 98.9 and 146.2, respectively indicated that it was adjacent to a nitrogen whose presence was demonstrated by HRMS/MS. The correlations from the mobile proton NH-11 to the olefinic carbons C-9, C-8 (δ_C 137.6) and C-12 (δ_C 129.8) and from the aromatic proton H-9 to C-8, C-10

and C-12 allowed to identify a pyrrole group. The HMBC correlation from methyl H_3-15 to the olefinic carbons C-8, C-7 (δ_C 123.9) and C-6 (δ_C 152.2) and from the hydroxy group OH-6 to C-7, C-6 and C-5 (δ_C 107.3) linked the pyrrole cycle to a phenol moiety. The HMBC correlations from the aromatic proton H-3 to C-5, C-4 (δ_C 160.5) and the ester carbon C-2 (δ_C 179.1) and from the methoxy to C-4 allowed to position a 2-pyrone cycle. The ROESY correlations from H-9 to the methyls H_3-16 and H_3-15 and from H-3 to the methoxy H_3-14 were in good agreement with 5-hydroxy-4-methoxy-6,8-dimethylpyrano[3,2-*g*]indol-2(9H)-one (Figure 4).

Compound **19** in F107, showed a Na^+ adduct ion at *m/z* 599.4380 which correlated to $C_{35}H_{60}O_6$. The NMR spectra of **19** indicated the presence of stigmast-8-en-3-ol with typical signals like two methyl singlets at δ_H 0.65 (3H, s, H_3-18) and 0.96 (3H, s, H_3-19), three methyl doublets at δ_H 0.79 (3H, d, *J*=6.9 Hz, H_3-27), 0.82 (3H, d, *J*=6.9 Hz, H_3-26), 0.90 (3H, d, *J*=6.5 Hz, H_3-21), one methyl triplet at δ_H 0.82 (3H, t, *J*=7.3 Hz, H_3-29), one oximethine at δ_H 3.46 (1H, tt, *J*=11.2, 4.3 Hz, H-3) and one olefinic carbons detected on the HMBC spectrum from the correlations of methyl H‘’-18 to C-9 (δ_C 140.4). Additional signals corresponding to a glucose unit were detected at δ_H 2.89 (1H, td, *J*=8.4, 4.8 Hz, H-2'), 3.01 (1H, td, *J*=9.2, 5.0 Hz, H-4'), 3.06 (1H, m, H-5'), 3.12 (1H, td, *J*=8.9, 4.8 Hz, H-3'), 3.40 (1H, m, H-6'b), 3.64 (1H, dd, *J*=11.1, 6.2 Hz, H-6'a), 4.22 (1H, d, *J*=7.8 Hz, H-1'). Due to the very small amount of isolated compound and the presence of an overlapping fatty acid in the fraction, it was not possible to obtain a complete assignment of the molecule. However, the ROESY correlation between the H-1' proton of glucose and the H-3 proton of the stigmasterol skeleton allowed the positioning of glucose in C-3 and to identify **19** as 3-*O*-β-D-glucopyranoside-stigmast-8-en-3-ol.

In addition to the compounds described in the polar part of the chromatogram (F1-27), F10 exhibited a ^{1}H-NMR spectrum of possibly 2 to 3 metabolites. The HRMS/MS data confirmed the presence of two ions at *m/z* 199.0965 and 155.0703 $[M + H]^+$ which are typical for $C_{10}H_{15}O_4$ and $C_8H_{11}O_3$ respectively.

A detailed 2D-NMR analysis of the fraction revealed the presence of 3 compounds which share a 3-methyl-pyran-2-one moiety similar to the one of **4** as indicated by the aromatic H-4 and H-5 at δ_H/δ_C 7.35-7.36/140.4-140.5 and 6.26-6.33/100.4-101.4, respectively and the methyl at δ_H/δ_C 1.95-1.96/16.0-16.2. Compounds **2a** and **2b** ($C_{10}H_{15}O_4$) were diastereoisomers with a 2,3-dihydroxybutan-2-yl side chain characterized by a methyl doublet (*J*=6.3 Hz, H_3-9) at δ_H 0.97 and 1.03, an oxygenated methine (m, H-8) at δ_H 3.73 and 3.74, and a methyl singlet (H_3-10) at δ_H 1.37 and 1.24 for **2a** and **2b**, respectively. The hydroxylation in C-7 and the linkage of the 2,3-dihydroxybutyl chain in C-6 was confirmed by the HMBC correlations from the methyl H_3-10 to C-6 (δ_C 167.0 and 167.2 for **2a** and **2b**, respectively), C-7 (δ_C 74.5 and 75.0 for **2a** and **2b**, respectively) and C-8 (δ_C 70.2 and 70.4 for **2a** and **2b**, respectively) and from the aromatic protons H-4 and H-5 to C-6. On the other hand, the 3-methyl-pyran-2-one of **3** ($C_8H_{11}O_3$) was substituted by a hydroxyethyl group in C-6 as indicated by the methyl doublet at δ_H 1.30 (3H, d, *J*=6.6 Hz, H_3-8), the methine at δ_H 4.41 (1H, q, *J*=6.6 Hz, H-7), and the HMBC correlation from the methyl to C-6 (δ_C 165.6) and C-7 (δ_C 64.9).

Overall, the combination of the LC-HRMS/MS data and *pseudo*-LC-NMR plot together with in depth 2D-NMR analysis of selected peaks provided a good overview of all main constituents of fractions F1-135 in a single semi-preparative HPLC separation. As many of the fractions were in very small quantities (in the sub-mg range), we had to find a strategy to collect enough compounds

for the bioassays which could only be conducted, after optimization, with at least 500 µg of pure compound.

2.7 Determination of bioactive zones

Following our workflow, to ensure accumulating enough material required for bioassays, the 135 collected fractions were pooled into 14 chromatographic zones (Z), where each zone represents 5 minutes window of elution time (Figure 6A). Submitting of the pooled fractions to bioactivity tests gives an approximate location of the active compounds and facilitates targeting them in an additional chromatographic separation. Since the extract was active against a methicillin-resistant *Staphylococcus aureus* (MRSA), the 14 zones were subjected firstly to MIC tests against this strain. As a result, only zone 9 (Z9) showed significant inhibitory effect at 32 µg/ml which suggested the presence of an antibacterial compound in fractions F81-91. In parallel, the 14 zones were evaluated for anti-QS of PA in the same way as for the crude extract and on the same reporter genes (*pqsA* and *lasB*).

For this purpose, we consider zones with bioactive candidates, those that have shown values of 70% or less in fluorescence level for at least one of the reporters. The value of 70% was chosen since each zone is still a mixture of several constituents and to avoid missing pure bioactive candidates. As a result, 7 zones from Z3-Z9, which represent the mid-polarity region, presented activity as QS inhibitors. Z5 was the most active one and significantly reduced the fluorescence level of gene *pqsA* to 31% and *lasB* to 43% (Table 3). In order to determine the specific molecules responsible for these activities, an additional LC-peak targeted chromatographic separation at semi-preparative level was performed, and an enrichment step was designed to remove the very lipophilic zones which clearly were not responsible for bioactivity.

2.8 Enrichment of the crude extract for targeted purification of bioactive compounds

In order to increase the concentration of the bioactive compounds in Z3-Z9, the ethyl acetate crude extract was submitted to liquid-liquid separation using water/methanol in ratio (7:3) and hexane. This yielded approximately 70 mg of hydroalcoholic fraction and 90 mg of hexane fraction from 160 mg of crude extract. As seen in Figure 6B-C, all zones of interest (Z3-9) are retained in the hydroalcoholic part except Z9 and the ELSD traces highlight well the efficiency of the enrichment procedure.

Taking into account the enrichment factor (2.3 folds), a single semi-preparative HPLC fractionation was carried on 30 mg of hydroalcoholic fraction in the same conditions as for the crude extract (Supplementary Figure S4). This yielded a good baseline separation in most compounds that ease the peak targeted collection. Purity of collected fractions were checked by ^{1}H-NMR and LC-ELSD-MS (data not shown) and enabled the bioactivity assessment of compounds **1-14**. Since Z9 was also a bioactive target, the apolar hexane fraction was purified similarly. Interestingly, by comparing the dry weights of collected fractions from enriched extract with the equivalent ones from crude extract all compounds were collected in amounts higher than 500 µg which was the threshold for the bioassay we selected. This grants supplementary amounts to perform further bioassay experiments such as quantitative PCR.

2.9 Biological assay of pure compounds

In order to assign compounds which are responsible for the antibacterial and anti-QS activity, purified compounds (**4**-**16**) that belong to Z3-Z9 were submitted to the same biological tests as described before.

For the QS test on *P. aeruginosa*, compounds **5**, **10**, **13** and **16**, presented moderate to weak activity profiles as they did not reach values under 30% in fluorescence reduction (Table 3) at 128 µg/ml. However, a mixture of the known *Fusarium* quinones fusarubin (**7**) and 3-*O*-methylfusarubin (**8**) which previously located in the active Z5, presented an enhanced and significant QS inhibition (12% and 15%) in pqs and las systems respectively at 128 µg/ml. To further confirm these results, we performed quantitative RT-PCR analyses on QS regulated genes *pqsA, lasB*, and *rhlA* involved in rhamnolipids production (Van Gennip et al., 2009). The relative expression of QS regulated gene *pqsA* in the presence of **7** and **8** was two times less expressed than the reference (Figure 7B). However, relative expression of *lasB* and *rhlA* did not show significant effects (data not shown) unlike results obtained by *gfp* transcriptional fusions (Table 3). In addition, since the zone Z9 was the only one showing MRSA inhibition activity, its main compound is one of the new pyrones **16** was evaluated against MRSA following the protocol of Wiegand et al. (2008). Compound **16** presented MIC at 32 µg/mL (Table 3).

On the whole series of the isolated compounds anti-QS assay for *S. aureus* on the reporter strain *rnaIII-lacZ* targeting the reporter gene *agr* were also performed following the method of (Nielsen et al., 2010). Compounds **5**, **10**, **13** and **16** presented a QS *rnaIII*-lacZ inhibition at 32 µg/ml showing fluorescence values less than 20% (Table 3). These results were confirmed by real time quantitative reverse transcription (RT-qPCR) in gene expression of *hla* and *hld,* both coding for QS regulated exotoxins (Figure 7A). Compared to the positive control, the antagonist auto-inducing peptide (AIP) from *Staphylococcus caprae*, all of these compounds show a better inhibition on *hla* gene expression which codes for the alpha-hemolysin. The tendency is the same for *hld* gene expression which codes for the delta-hemolysin, except for **16** that shows a less efficient effect with an inhibition of only 2-folds (Figure 7A).

3 Discussion

This comprehensive study of *F. petroliphilum* enables an unambiguous characterization of 22 compounds based on one single high resolution semi-preparative HPLC separation of the crude extract.

On the chemical profiling aspect, this typical fungal extract (ethyl acetate extract from solid culture) allows us to devise an integrated workflow that bridges in depth LC-HRMS/MS molecular networking with subsequent NMR analysis. This was achieved by systematic collection of NMR data from fractions of the semi-preparative HPLC separation. We define this process as "*pseudo*-LC-NMR" since it enables combining proton NMR spectra recorded in a common solvent in a single 2D plot. This way of processing highlights relationships between metabolites through common chemical shifts and generates plots that also provide semi-quantitative estimation of their amount in the extract. In a first instance, The ^{1}H-NMR data acquired for all fractions correlated well with the dereplication results obtained from the molecular networks. For most of the unannotated metabolites, full *de novo* structure assignment based on 2D-NMR and MS data obtained from the profiling efficiently enables the identification of new fungal NPs. The unambiguous structural assignment of most of the main metabolites also provides a valid set of standards which allows more extended annotations to be performed through molecular networking mainly based on

relationships that could be established between analogues (MN annotation propagation). However, in its current state, the proposed workflow still requires partial manual inspection/processing of both NMR and MS data. Future development of algorithms for connecting NMR information into molecular network would facilitate the efficiency of the full metabolome composition assessment process. Our study mainly highlights the potential of such data integration and demonstrates that with well optimized chromatographic conditions at the semi-preparative HPLC level, high quality spectral data can be efficiently generated in a restricted laboratory time frame.

On the bioactivity aspects, we could demonstrate that it is possible to take advantage of the same fractionation to evaluate bioactivity on several complementary assays for assessing anti-bacterial and anti-QS activity. In our case, one of the limiting factors being the sensitivity of the bioassay, an enrichment of the extract had to be performed to meet the requirements of the tests. The method proposed is however generic and could be applied to various natural extracts of medium polarity and to diverse types of bioassays. It enables the characterization of specific bioactive compounds and provides at the same time valuable data for in depth metabolome characterization of a given organism.

In the case of this specific study, among the 22 compounds unambiguously identified, 13 were never reported to our knowledge. This allowed a better characterization of composition of *F. petroliphilum* which is a rarely chemically studied member of the *F. solani* species complex. Our genetic investigation of this endophyte also enables its unambiguous identification and position this strain as a member of *F. solani* species complex. Several of the identified metabolites exhibited weak to moderate MIC value on a gram-positive MRSA and no growth inhibition on the gram-negative *P. aeruginosa*. However, an in-depth study of the QS activity of both strains through our selected assays revealed significant QS inhibition for some of the metabolites especially for the known fusarubins for which anti-QS activities were never reported. Using our workflow, we were also able to show that the generic fractionation obtained by semi-preparative HPLC allowed a consistent concentration of activity from the broad chromatographic zones to the active ingredients. This further demonstrates the advantage of such high-resolution fractionation profiling for tracking bioactivity. Based on this approach, we plan to further study the different endophytes found in *Posidonia*, which we identify as an interesting model for the study of the endophytic community.

4 Materials and Methods

4.1 Plant Material, fungal endophytes isolation and identification

Posidonia oceanica shoots were collected from the shores of Banyuls-sur-Mer in France at five to ten meters depth. Fresh plant parts (leaves, roots and rhizomes) were cleaned under stream water and then dipped into 70% ethanol for 3 minutes. Samples of all plant parts were cut into 1 cm^2 pieces and placed in a culture plate containing potato dextrose agar (PDA). Fungal tips were transferred to a new PDA culture plate as soon as they appeared and left to grow for 30 days.

Samples of the fungal cultures were sent to Bio2Mar, France (http://bio2mar.obs-banyuls.fr) who performed the amplification and sequencing of the internal transcribed spacers plus the 5.8S (ITS). After the removal of small and large subunit ITS flanking regions, a first identification of this fungal isolate was performed searching for similarity of that ITS sequences with those deposited in GenBank (National Center for Biotechnology Information; https://www.ncbi.nlm.nih.gov/pmc/articles/PMC5753231/). Sequence similarity search (BLAST;

https://blast.ncbi.nlm.nih.gov/Blast.cgi?PAGE_TYPE=BlastSearch#) in GenBank used the 'blastn' (Megablast) option excluding "uncultured/environmental sample sequences".

To identify more precisely the selected *Fusarium* strain FEP 16, DNA was extracted from a sample of the fungal culture placed in 500 µL of cetyl-trimethyl-ammonium bromide buffer (CTAB 1x). DNA extraction was performed according to Hofstetter et al. (2002). Four more loci were amplified and sequenced: part of the transcription elongation factor 1-alpha (*TEF*1-α) using primers EF1-1F and EF1-1R (Morehouse et al., 2003), part of the RNA polymerase II second largest subunit [*RPB2*] using primers fRPB2-5F and fRPB2-7cR for region 5-7 and fRPB2-7cF and fRPB2-11aR for region 7-11 (Liu et al., 1999), part of β-tubulin using primers Bt2a and Bt2b (Glass and Donaldson, 1995), and part of calmodulin with primers CAL-228F and CAL-737R (Carbone and Kohn, 2019). Amplification of these loci used reagents and conditions of the Taq PCR core kit (Qiagen Inc., Valencia, CA, USA). Sanger sequencing was performed with the amplification primers by Fasteris SA (Life Science Genesupport, Geneva, Switzerland). The obtained sequences were assembled in Sequencher v. 4.9 (Gene Codes Corp., USA). These sequences were combined with sequences sampled from Bohni et al. (2016). The alignments of sequences were done in MacClade v. 4.08a (Maddison and Maddison, 1989). Ambiguously aligned regions (mostly spliceosomal introns in protein-coding genes and gap regions in ribosomal loci) were excluded from phylogenetic analyses.

Searches for the most likely tree included three independent runs conducted in PhyML v. 3.0 (Guindon and Gascuel, 2003), with evolutionary model = GTR and other parameters estimated during the search. Bootstrap values (BS) were inferred based on 500 replicates using the same settings as for the search of the most likely tree. Branch support was considered significant when BS values were $\geq$ 70% (Alfaro et al., 2003).

4.2 Cultivation and extraction of *Fusarium petroliphilum*

Small scale (10 plates) and large scale (100 plates) cultivations were done in identical conditions. The fungi *F. petroliphilum* strain was cultivated in the laboratory using Sabouraud dextrose agar (CM0041, Oxoid), suspended in artificial sea water, then laid down on 8.5 cm Petri dishes at room temperature for 18 days (Ingredients in Supplementary Table S3) (Kour et al., 2007). After 18 days, the fresh agar was cut into 1 cm squares and directly agitated with ethyl acetate overnight. Agitation was repeated with fresh solvent three times followed by 20 minutes ultrasound sonication. The solvent was filtered then evaporated to dryness under vacuum to yield 300 mg of extract.

4.3 General Experimental Procedures

The NMR spectroscopic data were recorded on a Bruker Avance III HD 600 MHz. NMR spectrometer equipped with a QCI 5mm Cryoprobe and a SampleJet automated sample changer (Bruker BioSpin, Rheinstetten, Germany). Chemical shifts are measured in parts per million (δ) using the residual DMSO-d_6 (δ_H 2.50; δ_C 39.5) as internal standard for ^{1}H and ^{13}C, respectively, and coupling constants (*J*) are reported in Hz. Complete assignments were performed based on 2D-NMR experiments (COSY, ROESY, HSQC, and HMBC). Optical rotations were measured with a Jasco P-2000 polarimeter (JASCO Corporation, Tokyo, Japan). UV absorbance was measured with a JASCO FT/IR-4100 spectrometer (JASCO Corporation) equipped with a PIKE MIRacle™ (JASCO Corporation).

4.4 UHPLC-PDA-MS and UHPLC-HRMS/MS Analyses

UHPLC-PDA-MS analyses were performed on a Waters Acquity UHPLC, equipped with PDA and QDA detectors supplemented with electrospray ionization source (ESI). For the profile of the ethyl acetate extract, 3 µl was injected through a Waters® column BEH C18 (100 x 2.1 mm i.d.,1.7 µm, Waters, Milford, MA, USA). Solvent system was MeOH (B) and H_2O (A). The optimized conditions were as follows: 34% to 100% of B in 16.57 min., followed by 3 minutes to wash at 100% of B. Flow rate was 0.3 mL/min.

UHPLC-HRMS/MS analyses was performed on Thermo Dionex Ultimate 3000 UHPLC system interfaced with a Q Exactive Plus MS (Thermo Scientific, Bremen, Germany) supplemented with heated electrospray Ionization source (HESI-II). For the profile of the ethyl acetate extract, 2 µl of the extract was injected through a Waters® column BEH C18 100 x 2.1 mm, 1.7 µm i.d. Solvent system was MeCN (B) and H2O (A), both containing 0.1% FA. Gradient mode was as follows: 5% to 100% of B in 18 min, at flow rate of 0.6 mL/min. followed by 4 min. for washing and reconditioning. For the short run analyses of all fractions, 2 µl was injected through a Waters® column BEH C18 (50 x 2.1 mm i.d.,1.7 µm, Waters, Milford, MA, USA). Solvent system was MeCN (B) and H_2O (A), both containing 0.1% FA. Gradient mode was 5% to 100% of B in 4 min., followed by 2 min. for washing and reconditioning.

4.5 Generation of molecular networks

Raw spectral data of the extract were analyzed by MZmine 2.53 (Pluskal et al., 2010). The parameters were adjusted as follows: Mass detection performed as MS level 1 (noise level at $1e^6$) and MS level 2 (noise level at 0). ADAP chromatogram builder was used with threshold set to $4e^5$. Chromatogram deconvolution (algorithm ADAP) set within its default parameters except for RT wavelet range set as 0 to 0.1. The most intense isotopes were kept through isotope peak grouper. Adduct search was performed for (Na^+, K^+, NH_4^+, ACN^+) in PI and (Na^-, K^-) in NI. Custom database search restricted to *Fusarium* was performed using the Dictionary of Natural Products. Peak alignment was performed using join aligner method where absolute RT tolerance at 0.03 minutes. Molecular networks built through GNPS (https://gnps.ucsd.edu/) and visualized using Cytoscape version 3.8.

4.6 HPLC-PDA analysis

HPLC-PDA analyses were conducted on a HP 1260 system equipped with a photodiode array detector (Agilent Technologies, Santa Clara, CA, USA). The HPLC conditions were as follows: X-Bridge C18 column (250 × 4.6 mm i.d., 5 µm, Waters, Milford, MA, USA); solvent system MeOH (B) and H_2O (A), both containing 0.1% FA. The optimized separation was performed in gradient mode as follows: 34% to 100% of B in 60 min. Flow rate 1 mL/min; injection volume 10 µL, sample concentration 10 mg/mL in the mobile phase. The ELSD detection parameters, pressure 3.4 bar, 45 °C, split to provide a 500 µL/min flow rate, gain 8.

4.7 Generation of 2D plot

The aligned ^{1}H-NMR spectra of all 135 fractions were divided into equally sized bins (0.01 ppm) in a range from -1 to 15 ppm then exported as excel file (.csv). The file was loaded into an R script which was written to create an interactive 2D plot that combines all binned spectra in a matrix (sample Vs. ppm). The retention time was added manually to the plot. The following R packages were used: “plotly”, “stringr”, “reshape2”, “dplyr” and “readr”. The R script is freely available here (https://github.com/oolonek/pseudo_lcnmr_plotter/blob/main/src/plotter/NMR_data_plotter.Rmd).

4.8 Liquid/liquid extraction and extract purification at semi-preparative scale

The crude was subjected to liquid/liquid extraction, 160 mg was suspended in 50 ml 7:3 water/methanol, the same volume of hexane was added to the suspension and gently shacked, the apolar phase was transferred to new flask, the later step was repeated 4 times. Both fractions were dried under vacuum, the hydroalcoholic fraction yield was 70 mg and 90 mg for hexane fraction. Both fractions plus the original crude extract were purified using a semi-preparative HPLC-UV equipment (Shimadzu® SPD-20A, Kyoto, Japan) through an X-Bridge RP C18 column (250 x 19 mm i.d., 5 µm. To transfer from analytical to semi-preparative HPLC, the conditions were geometrically transferred by selecting a column with a similar stationary phase and gradient system (Guillarme et al., 2008). The flow rate was set at 17 mL/min. In order to avoid loss of resolution, the sample was introduced into the column through a homemade dry load cell (Queiroz et al., 2019). All peaks have been collected automatically by UV threshold at 254 nm or ELSD trace. After collection, each fraction was evaporated to dryness using a high-performance evaporation system (HT-4X Genevac®, Stone Ridge, NY, USA).

4.9 Description of the isolated compounds

Adenosine (1): white amorphous solid (0.3 mg); ^{1}H-NMR (DMSO-d_6, 600 MHz) δ 3.55 (1H, dd, *J*=12.1, 3.5 Hz, H-5'b), 3.67 (2H, dd, *J*=12.1, 3.5 Hz, H-5'a), 3.96 (2H, q, *J*=3.4 Hz, H-4'), 4.14 (1H, dd, *J*=4.8, 3.1 Hz, H-3'), 4.60 (1H, t, *J*=5.6 Hz, H-2'), 5.87 (1H, d, *J*=6.3 Hz, H-1'), 7.33 (1H, s, OH-5), 8.13 (1H, s, H-7), 8.34 (1H, s, H-2); ^{13}C-NMR (DMSO-d_6, 151 MHz) δ 61.6 (C-5'), 70.6 (C-3'), 73.4 (C-2'), 85.8 (C-4'), 87.8 (C-1'), 119.3 (C-4), 139.8 (C-2), 156.1 (C-5). HRMS/MS *m/z* 268.1033 $[M + H]^+$ (calcd for $C_{10}H_{14}N_5O_4$, 268.1045).

6-(2,3-dihydroxybutan-2-yl)-3-methyl-2H-pyran-2-one (**2**): white amorphous solid; **2a**: ^{1}H-NMR (DMSO-d_6, 600 MHz) δ 0.97 (3H, d, *J*=6.3 Hz, H_3-9), 1.31 (3H, s, H_3-10), 1.95 (3H, d, *J*=1.2 Hz, H_3-11), 3.73 (1H, m, H-8), 4.67 (1H, d, *J*=6.1 Hz, OH-8), 5.19 (1H, s, OH-7), 6.32 (1H, d, *J*=5.7 Hz, H-5), 7.35 (1H, m, H-4); ^{13}C-NMR (DMSO-d_6, 151 MHz) δ 16.0 (C-11), 17.4 (C-9), 21.8 (C-10), 70.2 (C-8), 74.5 (C-7), 101.4 (C-5), 121.3 (C-3), 140.4 (C-4), 162.7 (C-2), 167.0 (C-6); **2b**: ^{1}H-NMR (DMSO-d_6, 600 MHz) δ 1.03 (2H, d, *J*=6.4 Hz, H_3-9), 1.24 (3H, s, H_3-10), 1.95 (3H, d, *J*=1.2 Hz, H_3-11), 3.74 (1H, m, H-8), 4.59 (1H, d, *J*=5.8 Hz, OH-8), 5.09 (1H, s, OH-7), 6.33 (1H, d, *J*=5.8 Hz, H-5), 7.35 (1H, m, H-4); ^{13}C-NMR (DMSO-d_6, 151 MHz) δ 16.0 (C-11), 17.1 (C-9), 22.6 (C-10), 70.4 (C-8), 75.0 (C-7), 101.4 (C-5), 120.9 (C-3), 140.4 (C-4), 162.7 (C-2), 167.2 (C-6). HRMS/MS *m/z* 199.0962 $[M + H]^+$ (calcd for $C_{10}H_{15}O_4$, 199.0966).

6-(1-hydroxyethyl)-3-methyl-2H-pyran-2-one (**3**): white amorphous solid; ^{1}H-NMR (DMSO-d_6, 600 MHz) δ 1.30 (3H, d, *J*=6.6 Hz, H_3-8), 1.96 (3H, d, *J*=1.2 Hz, H_3-9), 4.41 (1H, q, *J*=6.6 Hz, H-7), 5.56 (1H, d, *J*=4.4 Hz, OH-7), 6.26 (1H, dd, *J*=6.7, 0.8 Hz, H-5), 7.36 (1H, m, H-4); ^{13}C-NMR (DMSO-d_6, 151 MHz) δ 16.2 (C-9), 21.5 (C-8), 64.9 (C-7), 100.4 (C-5), 122.0 (C-3), 140.5 (C-4), 162.7 (C-2), 165.6 (C-6). HRMS/MS *m/z* 155.0703 $[M + H]^+$ (calcd for $C_8H_{11}O_3$, 155.0708).

Gibepyrone D (**4**): pale yellow amorphous solid (0.5 mg); ^{1}H-NMR (DMSO-d_6, 600 MHz) δ 2.03 (3H, d, *J*=1.3 Hz, H_3-10), 2.27 (3H, s, H_3-11), 6.43 (1H, s, H-8), 6.72 (1H, d, *J*=6.9 Hz, H-5), 7.44 (1H, dd, *J*=6.9, 1.3 Hz, H-4); ^{13}C-NMR (DMSO-d_6, 151 MHz) δ 12.9 (C-11), 16.2 (C-10), 105.6 (C-5), 125.8 (C-3), 139.8 (C-4), 156.6 (C-6), 161.4 (C-2). HRMS/MS *m/z* 195.1016 $[M + H]^+$ (calcd for $C_{10}H_{11}O_4$, 195.0657).

Aloesol (**5**): milk white crystals (0.3 mg); ^{1}H-NMR (DMSO-d_6, 600 MHz) δ 1.14 (3H, d, *J*=6.2 Hz, H_3-14), 2.54 (1H, dd, *J*=14.3, 7.7 Hz, H-12b), 2.60 (1H, dd, *J*=14.3, 5.2 Hz, H-12a), 2.65 (3H, s, H_3-11), 4.02 (1H, dq, *J*=7.6, 5.5 Hz, H-13), 4.83 (1H, d, *J*=5.1 Hz, OH-13), 5.96 (1H, s, H-3), 6.60 (1H, d, *J*=2.4 Hz, H-6), 6.62 (1H, d, *J*=2.4 Hz, H-8); ^{13}C-NMR (DMSO-d_6, 151 MHz) δ 22.3 (C-11), 23.3 (C-14), 42.7 (C-12), 63.9 (C-13), 100.4 (C-8), 111.4 (C-3), 114.3 (C-10), 116.3 (C-6), 141.3 (C-5), 159.1 (C-7), 160.8 (C-9), 164.6 (C-2). HRMS/MS *m/z* 235.0963 $[M + H]^+$ (calcd for $C_{13}H_{15}O_4$, 235.0965).

5-hydroxy-4-(hydroxymethyl)-8-methoxy-2-methyl-1H-benzo[*g*]indole-6,9-dione (**6**): pale rose amorphous solid (0.2 mg); UV λ_{max} 213, 280 nm; ^{1}H-NMR (DMSO-d_6, 600 MHz) δ 2.44 (3H, d, *J*=1.0 Hz, H_3-14), 3.89 (3H, s, H_3-16), 4.75 (2H, d, *J*=5.5 Hz, H_2-15), 5.06 (1H, t, *J*=5.6 Hz, OH-15), 6.23 (1H, s, H-3), 6.44 (1H, dd, *J*=2.1, 1.1 Hz, H-11), 11.39 (1H, s, H-13), 12.88 (1H, s, OH-5); ^{13}C-NMR (DMSO-d_6, 151 MHz) δ 13.8 (C-14), 55.1 (C-15), 56.6 (C-16), 99.8 (C-11), 107.4 (C-10), 109.0 (C-3), 126.8 (C-6), 130.5 (C-8), 137.5 (C-7), 146.7 (C-12), 152.1 (C-5), 160.5 (C-2), 179.5 (C-1), 191.0 (C-4); HRMS/MS *m/z* 288.0846 $[M + H]^+$ (calcd for $C_{15}H_{14}NO_5$, 288.0866).

Fusarubin (**7**): Reddish rose crystals; ^{1}H-NMR (DMSO-d_6, 600 MHz) δ 1.48 (3H, s, H_3-11), 2.59 (1H, m, H-4''), 2.78 (1H, dd, *J*=18.0, 1.9 Hz, H-4'), 3.91 (3H, s, H_3-12), 4.67 (1H, dt, *J*=17.5, 2.4 Hz, H-1''), 4.72 (1H, d, *J*=17.5 Hz, H-1'), 6.13 (1H, d, *J*=1.6 Hz, OH-3), 6.46 (1H, s, H-8), 12.49 (1H, s, OH-5), 13.00 (1H, s, OH-10); ^{13}C-NMR (DMSO-d_6, 151 MHz) δ 28.4 (C-11), 32.8 (C-4), 57.0 (C-12), 57.3 (C-1), 92.9 (C-3), 107.1 (C-9a), 109.7 (C-8), 133.3 (C-4a), 136.7 (C-10a), 156.3 (C-10), 159.6 (C-5), 160.7 (C-7), 177.8 (C-6), 184.7 (C-9). HRMS/MS *m/z* 307.0823 $[M + H]^+$ (calcd for $C_{15}H_{15}O_7$, 307.0812).

3-*O*-methylfusarubin (**8**): Reddish rose crystals; ^{1}H-NMR (DMSO-d_6, 600 MHz) δ 1.47 (3H, s, H_3-11), 2.67 (1H, dt, *J*=18.0, 1.9 Hz, H-4''), 2.85 (1H, dd, *J*=18.0, 2.0 Hz, H-4'), 3.20 (3H, s, H_3-13), 3.91 (3H, s, H_3-12), 4.44 (1H, dt, *J*=17.7, 2.5 Hz, H-1''), 4.78 (1H, d, *J*=17.7 Hz, H-1'), 6.45 (1H, s, H-8), 12.49 (1H, s, OH-5), 12.99 (1H, s, OH-10); ^{13}C-NMR (DMSO-d_6, 151 MHz) δ 22.4 (C-11), 32.5 (C-4), 48.3 (C-13), 57.0 (C-12), 57.9 (C-1), 96.3 (C-3), 109.7 (C-8), 132.1 (C-4a), 135.7 (C-10a), 155.4 (C-10), 158.7 (C-5), 160.7 (C-7), 178.4 (C-6), 185.1 (C-9). HRMS/MS *m/z* 319.0976 $[M - H]^-$ (calcd for $C_{16}H_{15}O_7$, 319.0817).

(6E)-7-(4-methoxy-6-oxo-6H-pyran-2-yl)-3,5-dimethyloct-6-enoic acid (**9**): Red amorphous solid (0.4 mg); $[\alpha]^{20}_D$ +22.3 (c 0.04, MeOH);UV (DAD) λ_{max} 218, 269; ^{1}H-NMR (DMSO-d_6, 600 MHz) δ 0.89 (3H, d, *J*=6.6 Hz, H_3-14), 0.96 (3H, d, *J*=6.6 Hz, H_3-15), 1.21 (1H, dt, *J*=13.4, 7.4 Hz, H-10''), 1.34 (1H, dt, *J*=13.4, 6.8 Hz, H-10'), 1.79 (1H, dqd, *J*=8.5, 6.8, 5.1 Hz, H-11), 1.86 (3H, d, *J*=1.4 Hz, H_3-16), 1.96 (1H, dd, *J*=15.0, 8.5 Hz, H-12''), 2.25 (1H, m, H-12'), 2.67 (1H, m, H-9), 3.88 (3H, s, H_3-17), 5.52 (1H, d, *J*=1.8 Hz, H-3), 6.11 (1H, d, *J*=1.8 Hz, H-5), 6.15 (1H, dd, *J*=9.8, 1.4 Hz, H-8), 11.99 (1H, s, COOH); ^{13}C-NMR (DMSO-d_6, 151 MHz) δ 12.3 (C-16), 19.8 (C-14), 19.9 (C-15), 27.6 (C-11), 29.9 (C-9), 40.9 (C-12), 43.3 (C-10), 56.4 (C-17), 88.7 (C-3), 108.7 (C-5), 124.3 (C-7), 140.0 (C-8), 159.6 (C-6), 167.2 (C-4), 173.7 (C-13), 180.2 (C-2). HRMS/MS *m/z* 295.1542 $[M + H]^+$ (calcd for $C_{16}H_{23}O_5$, 295.1545).

6-((*E*)-6-ethyl-7-hydroxy-4-methylhept-2-en-2-yl)-4-methoxy-2H-pyran-2-one (**10**): Red amorphous solid (0.7 mg); $[\alpha]^{20}_D$ +82.7 (c 0.03, MeOH); UV (DAD) λ_{max} 286, 422; ^{1}H-NMR (DMSO-d_6, 600 MHz) δ 0.81 (3H, t, *J*=7.3 Hz, H_3-13), 0.98 (3H, d, *J*=6.6 Hz, H_3-15), 1.22 (1H, m, H-10''), 1.23 (1H, m, H-11), 1.27 (2H, m, H_2-12), 1.35 (1H, m, H-10'), 1.86 (3H, d, *J*=1.3 Hz, H_3-16), 2.69 (1H, m, H-9), 3.25 (1H, dt, *J*=10.2, 5.0 Hz, H-14''), 3.30 (1H, dt, *J*=10.2, 5.0 Hz, H-14'),

3.88 (3H, s, H_3-17), 4.34 (1H, t, *J*=5.2 Hz, OH-14), 5.52 (1H, d, *J*=1.8 Hz, H-3), 6.10 (1H, d, *J*=1.8 Hz, H-5), 6.14 (1H, dd, *J*=9.9, 1.5 Hz, H-8); ^{13}C-NMR (DMSO-d_6, 151 MHz) δ 10.5 (C-13), 12.1 (C-16), 20.4 (C-15), 22.6 (C-12), 29.9 (C-9), 37.8 (C-10), 39.1 (C-11), 56.3 (C-17), 62.9 (C-14), 88.6 (C-3), 108.6 (C-5), 124.1 (C-7), 140.4 (C-8), 159.6 (C-6), 167.2 (C-4), 180.2 (C-2). HRMS/MS *m/z* 281.1745 $[M + H]^+$, calcd for $C_{16}H_{25}O_4$, 281.1747.

Bostrycoidin (**11**): Dark red amorphous solid (0.5 mg); ^{1}H-NMR (DMSO-d_6, 600 MHz) δ 2.73 (3H, s, H_3-15), 3.98 (3H, s, H_3-16), 7.04 (1H, s, H-7), 7.98 (1H, s, H-4), 9.33 (1H, s, H-1), 12.87 (1H, s, OH-5/8), 13.54 (1H, s, OH-5/8); ^{13}C-NMR (DMSO-d_6, 151 MHz) δ 24.5 (C-15), 56.7 (C-16), 107.8 (C-7), 117.5 (C-4), 124.0 (C-13), 138.4 (C-14), 147.9 (C-1), 157.6 (C-6), 164.8 (C-3). HRMS/MS *m/z* 286.0715 $[M + H]^+$ (calcd for $C_{15}H_{12}NO_5$, 286.0716).

5β,6β-23,26-diepoxy-3β,7α,9α-trihydroxy-(20Z,23S,24S,25R)ergosta-8(14),20-dien-15-one (**12**): pale yellow amorphous solid (0.4 mg); $[\alpha]^{20}_D$ +18.9 (c 0.04, MeOH); UV λ_{max} 248, 229, 229; ^{1}H-NMR (DMSO-d_6, 600 MHz) δ 0.77 (3H, s, H_3-18), 0.85 (3H, d, *J*=7.0 Hz, H_3-28), 0.89 (3H, s, H_3-19), 0.90 (3H, d, *J*=6.8 Hz, H_3-26), 1.20 (1H, dt, *J*=13.6, 3.3 Hz, H-4α), 1.45 (3H, m, H-1β, H-2β, H-11α), 1.66 (2H, m, H_2-12), 1.69 (1H, m, H-11β), 1.73 (3H, d, *J*=1.2 Hz, H_3-21), 1.85 (2H, m, H-2α, H-24), 2.00 (1H, td, *J*=14.4, 4.0 Hz, H-1α), 2.06 (1H, dd, *J*=13.6, 11.5 Hz, H-4β), 2.16 (1H, dd, *J*=18.3, 7.3 Hz, H-16α), 2.26 (1H, m, H-25), 2.35 (1H, m, H-17), 2.63 (1H, m, H-16β), 3.27 (1H, d, *J*=3.7 Hz, H-6), 3.59 (1H, tq, *J*=10.6, 5.0 Hz, H-3), 3.93 (1H, dd, *J*=8.2, 6.4 Hz, H-27'), 4.18 (1H, t, *J*=8.5 Hz, H-23), 4.77 (1H, d, *J*=5.0 Hz, OH-3), 4.77 (1H, d, *J*=2.3 Hz, OH-9), 4.91 (1H, d, *J*=5.2 Hz, OH-7), 5.22 (1H, d, *J*=8.4 Hz, H-22), 5.53 (1H, dd, *J*=5.2, 3.7 Hz, H-7); ^{13}C-NMR (DMSO-d_6, 151 MHz) δ 11.2 (C-28), 13.5 (C-26), 17.6 (C-18), 18.8 (C-21), 19.8 (C-19), 25.6 (C-1), 26.7 (C-11), 30.2 (C-2), 32.1 (C-12), 35.9 (C-25), 37.0 (C-10), 39.5 (C-16), 39.9 (C-4), 42.9 (C-24), 43.1 (C-13), 51.5 (C-17), 59.7 (C-7), 60.4 (C-6), 66.5 (C-3), 68.1 (C-5), 73.7 (C-27), 74.8 (C-9), 79.7 (C-23), 128.1 (C-22), 134.1 (C-20), 142.8 (C-14), 206.7 (C-15). HRMS/MS *m/z* 473.2877 $[M + H]^+$ (calcd for $C_{28}H_{41}O_6$, 473.2903).

2-(2,3,5,6,7,7a-hexahydro-1-((*E*)-6-hydroxy-5,6-dimethylhept-3-en-2-yl)-7a-methyl-5-oxo-1H-inden-4-yl)acetic acid (**13**): pale yellow amorphous solid (0.4 mg); $[\alpha]^{20}_D$ +21.5 (c 0.04, MeOH); UV λ_{max} 247, 207; ^{1}H-NMR (DMSO, 600 MHz) δ 0.92 (3H, d, *J*=7.0 Hz, H_3-21), 0.99 (3H, s, H_3-20), 1.03 (3H, d, *J*=7.1 Hz, H_3-14), 1.03 (3H, s, H_3-19), 1.06 (3H, s, H_3-12), 1.42 (1H, m, H-11), 1.50 (1H, m, H-10''), 1.78 (1H, m, H-10'), 1.79 (1H, m, H-6''), 2.01 (1H, p, *J*=7.0 Hz, H-17), 2.16 (1H, m, H-6'), 2.17 (1H, m, H-13), 2.19 (1H, m, H-5''), 2.22 (1H, m, H-5'), 2.99 (1H, d, *J*=16.5 Hz, H-2''), 3.02 (1H, d, *J*=16.5 Hz, H-2'), 5.26 (1H, dd, *J*=15.3, 8.7 Hz, H-15), 5.41 (1H, dd, *J*=15.3, 7.0 Hz, H-16); ^{13}C-NMR (DMSO-d_6, 151 MHz) δ 14.9 (C-21), 16.2 (C-12), 20.8 (C-14), 26.0 (C-19), 27.0 (C-10), 28.2 (C-20), 30.8 (C-2), 32.7 (C-5), 35.8 (C-6), 38.1 (C-13), 44.7 (C-7), 47.1 (C-17), 55.5 (C-11), 70.5 (C-18), 131.1 (C-16), 135.0 (C-15), 171.7 (C-1), 175.2 (C-8). HRMS/MS *m/z* 349.2383 $[M + H]^+$ (calcd for $C_{21}H_{33}O_4$, 349.2378).

2-(2,3,5,6,7,7a-hexahydro-1-((*E*)-7-hydroxy-5,6-dimethylhept-3-en-2-yl)-7a-methyl-5-oxo-1H-inden-4-yl)acetic acid (**14**): pale yellow amorphous solid (0.3 mg); $[\alpha]^{20}_D$ +19.8 (c 0.07, MeOH); UV λ_{max} 245, 212; ^{1}H-NMR (DMSO-d_6, 600 MHz) δ 0.75 (3H, d, *J*=6.9 Hz, H_3-19), 0.94 (3H, d, *J*=7.0 Hz,H_3- 21), 1.03 (3H, d, *J*=6.7 Hz, H_3-14), 1.06 (3H, s, H_3-12), 1.41 (1H, m, H-11), 1.43 (1H, m, H-18), 1.51 (1H, m, H-10''), 1.78 (2H, m, H-6'', H-10'), 2.17 (3H, m, H-6', H-13, H-17), 2.22 (1H, m, H-5''), 2.98 (1H, d, *J*=16.4 Hz, H-2''), 3.02 (1H, d, *J*=16.4 Hz, H-2'), 3.17 (1H, m, H-20), 5.27 (2H, m, H-15, H-16); ^{13}C-NMR (DMSO-d_6, 151 MHz) δ 13.1 (C-19), 16.3 (C-12), 18.3 (C-21), 21.0 (C-14), 27.3 (C-10), 30.9 (C-2), 32.7 (C-5), 35.9 (C-6), 37.0 (C-17), 38.2 (C-13), 40.6 (C-

18), 44.6 (C-7), 55.5 (C-11), 64.4 (C-20), 130.9 (C-16), 135.0 (C-15), 171.8 (C-1), 175.2 (C-8). HRMS/MS *m/z* 349.2349 $[M + H]^+$ (calcd for $C_{21}H_{33}O_4$, 349.2378).

5-hydroxy-4-methoxy-6,8-dimethylpyrano[3,2-*g*]indol-2(9H)-one (**15**): pale yellow amorphous (0.1 mg) solid; UV λ_{max} 280, 239; ^{1}H-NMR (DMSO-d_6, 600 MHz) δ 2.36 (3H, s, H_3-15), 2.44 (3H, s, H_3-16), 3.89 (3H, s, H_3-14), 6.21 (1H, s, H-3), 6.28 (1H, s, H-9), 11.39 (1H, s, NH-11), 12.84 (1H, s, OH-6); ^{13}C-NMR (DMSO-d_6, 151 MHz) δ 12.0 (C-15), 13.8 (C-16), 56.6 (C-14), 98.9 (C-9), 107.3 (C-5), 108.8 (C-3), 123.9 (C-7), 129.8 (C-12), 137.6 (C-8), 146.2 (C-10), 152.2 (C-6), 160.5 (C-4), 179.1 (C-2). HRMS/MS *m/z* 258.0771 $[M + H]^+$, calcd for $C_{14}H_{12}NO_4$, 258.0766.

4-methoxy-6-((*E*)-4,6-dimethyloct-2-en-2-yl)-2H-pyran-2-one (**16**): light brown amorphous solid (0.1 mg); $[\alpha]^{20}_D$ +17.5 (c 0.04, MeOH); UV λ_{max} 220,274; ^{1}H-NMR (DMSO-d_6, 600 MHz) δ 0.82 (3H, t, *J*=7.4 Hz, H_3-13), 0.84 (3H, d, *J*=6.3 Hz, H_3-14), 0.96 (3H, d, *J*=6.5 Hz, H_3-15), 1.08 (1H, m, H-12''), 1.14 (1H, m, H-10''), 1.32 (3H, m, H-10', H-11, H-12'), 1.86 (3H, d, *J*=1.2 Hz, H_3-16), 2.66 (1H, m, H-9), 3.88 (3H, s, H_3-17), 5.52 (1H, d, *J*=1.8 Hz, H-3), 6.10 (1H, d, *J*=1.8 Hz, H-5), 6.16 (1H, dq, *J*=9.8, 1.2 Hz, H-8); ^{13}C-NMR (DMSO-d_6, 151 MHz) δ 11.0 (C-13), 12.3 (C-16), 19.3 (C-14), 20.1 (C-15), 28.6 (C-12), 30.1 (C-9), 31.5 (C-11), 43.5 (C-10), 56.3 (C-17), 88.8 (C-3), 108.9 (C-5), 124.2 (C-7), 140.5 (C-8), 159.7 (C-6), 167.4 (C-4). HRMS/MS *m/z* 265.1816 $[M + H]^+$, calcd for $C_{16}H_{25}O_3$, 265.1803.

4-methoxy-3-methyl-6-((*E*)-4,6-dimethyloct-2-en-2-yl)-2H-pyran-2-one (**17**): light brown amorphous solid (0.1 mg); $[\alpha]^{20}_D$ +19.7 (c 0.04, MeOH); UV λ_{max} 218, 252; ^{1}H-NMR (DMSO-d_6, 600 MHz) δ 0.83 (3H, t, *J*=7.4 Hz, H_3-13), 0.85 (3H, d, *J*=6.1 Hz, H_3-14), 0.98 (3H, d, *J*=6.7 Hz, H_3-15), 1.24 (1H, m, H-12''), 1.34 (2H, m, H-11, H-12'), 1.69 (3H, s, H_3-18), 1.88 (3H, d, *J*=1.3 Hz, H_3-16), 2.66 (1H, m, H-9), 4.02 (3H, s, H_3-17), 6.17 (1H, s, H-5), 6.19 (1H, d, *J*=9.4 Hz, H-8); ^{13}C-NMR (DMSO-d_6, 151 MHz) δ 6.5 (C-18), 11.1 (C-13), 12.3 (C-16), 19.3 (C-14), 20.1 (C-15), 28.7 (C-12), 30.1 (C-9), 31.4 (C-11), 43.5 (C-10), 56.0 (C-17), 98.9 (C-3), 108.3 (C-5), 124.4 (C-7), 140.1 (C-8), 158.3 (C-6), 162.0 (C-4), 179.7 (C-2). HRMS/MS *m/z* 279.1967 $[M + H]^+$ (calcd for $C_{17}H_{27}O_3$, 279.1955).

2-(2,3,5,6,7,7a-hexahydro-7a-methyl-1-((*E*)-5,6-dimethylhept-3-en-2-yl)-5-oxo-1H-inden-4-yl)acetic acid (**18**): pale yellow amorphous solid (0.6 mg); $[\alpha]^{20}_D$ +14.9 (c 0.05, MeOH); UV λ_{max} 246, 239; ^{1}H-NMR (DMSO-d_6, 600 MHz) δ 0.81 (3H, d, *J*=6.9 Hz, H_3-20), 0.83 (3H, d, *J*=6.9 Hz, H_3-19), 0.91 (3H, d, *J*=6.7 Hz, H_3-21), 1.03 (3H, d, *J*=6.6 Hz, H_3-14), 1.06 (3H, s, H_3-12), 1.42 (1H, m, H-11), 1.48 (1H, m, H-18), 1.51 (1H, m, H-10''), 1.78 (1H, m, H-10'), 1.79 (1H, m, H-6''), 1.88 (1H, m, H-17), 2.15 (1H, m, H-6'), 2.18 (1H, m, H-13), 2.22 (1H, m, H-5''), 2.34 (1H, m, H-9''), 2.46 (1H, m, H-9'), 2.56 (1H, m, H-5'), 2.98 (1H, d, *J*=16.5 Hz, H-2''), 3.02 (1H, d, *J*=16.5 Hz, H-2'), 5.25 (1H, dd, *J*=15.2, 7.9 Hz, H-15), 5.29 (1H, dd, *J*=15.2, 7.0 Hz, H-16); ^{13}C-NMR (DMSO-d_6, 151 MHz) δ 16.3 (C-12), 17.3 (C-21), 19.4 (C-20), 19.7 (C-19), 20.9 (C-14), 27.2 (C-10), 27.3 (C-9), 32.4 (C-18), 32.7 (C-5), 35.8 (C-6), 38.1 (C-13), 42.0 (C-17), 44.6 (C-7), 55.4 (C-11), 125.0 (C-3), 132.0 (C-16), 134.7 (C-15), 171.7 (C-1), 175.2 (C-8), 196.3 (C-4). HRMS/MS *m/z* 333.2426 $[M + H]^+$ (calcd for $C_{21}H_{33}O_3$, 333.2429).

3-*O*-*β*-D-glucopyranoside-Stigmast-8-en-3-ol (**19**): pale yellow amorphous solid (0.1 mg); $[\alpha]^{20}_D$ +6.2 (c 0.08, MeOH); UV λ_{max} 234, 207; ^{1}H-NMR (DMSO-d_6, 600 MHz) δ 0.65 (3H, s, H_3-18), 0.79 (3H, d, *J*=6.9 Hz, H_3-27), 0.82 (3H, d, *J*=6.9 Hz, H_3-26), 0.82 (3H, t, *J*=7.3 Hz, H_3-29), 0.88 (1H, m, H-5), 0.90 (3H, d, *J*=6.5 Hz, H_3-21), 0.91 (1H, m, H-24), 0.96 (3H, s, H_3-19), 0.97 (2H, m, H-1b, H-14), 1.01 (1H, m, H-22b), 1.09 (1H, m, H-17), 1.20 (1H, m, H-28b), 1.25 (1H, m,

H-28a), 1.30 (1H, m, H-22a), 1.33 (1H, m, H-20), 1.47 (1H, m, H-2b), 1.63 (1H, m, H-25), 1.79 (1H, m, H-1a), 1.80 (3H, s), 2.12 (1H, t, *J*=12.5 Hz, 4''), 1.81 (1H, m, H-2a), 2.12 (1H, m, H-4b), 2.37 (1H, m, H-4a), 2.89 (1H, td, *J*=8.4, 4.8 Hz, H-2'), 3.01 (1H, td, *J*=9.2, 5.0 Hz, H-4'), 3.06 (1H, m, H-5'), 3.12 (1H, td, *J*=8.9, 4.8 Hz, H-3'), 3.40 (1H, m, H-6'b), 3.46 (1H, tt, *J*=11.2, 4.3 Hz, H-3), 3.64 (1H, dd, *J*=11.1, 6.2 Hz, H-6'a), 4.22 (1H, d, *J*=7.8 Hz, H-1'), 4.42 (1H, t, *J*=5.8 Hz, OH-6'), 4.85 (1H, d, *J*=5.0 Hz, OH-4'), 4.86 (1H, d, *J*=4.8 Hz, OH-2'), 4.88 (1H, d, *J*=4.8 Hz, OH-3'); ^{13}C-NMR (DMSO-d_6, 151 MHz) δ 11.6 (C-18), 11.8 (C-29), 18.6 (C-21), 19.0 (C-27), 19.1 (C-19), 19.6 (C-26), 22.5 (C-28), 28.7 (C-25), 29.3 (C-2), 33.3 (C-22), 35.4 (C-20), 36.3 (C-10), 36.7 (C-1), 38.3 (C-4), 39.1 (C-12), 41.8 (C-13), 45.1 (C-24), 49.6 (C-5), 55.4 (C-17), 56.1 (C-14), 61.0 (C-6'), 70.1 (C-4'), 73.4 (C-2'), 76.7 (C-5'), 76.8 (C-3, C-3'), 100.7 (C-1'), 140.4 (C-9). HRMS/MS *m/z* 599.4280 $[M + Na]^+$, calcd for $C_{35}H_{59}O_6Na$, 599.4287.

Cerevisterol (**20**)**:** White amorphous solid (0.9 mg) ^{1}H-NMR (DMSO-d_6, 600 MHz) δ 0.55 (3H, s, H_3-18), 0.80 (3H, d, *J*=7.3 Hz, H_3-27), 0.81 (3H, d, *J*=7.3 Hz, H_3-26), 0.88 (3H, d, *J*=6.8 Hz, H_3-28), 0.90 (3H, s, H_3-19), 0.99 (3H, d, *J*=6.5 Hz, H_3-21), 3.37 (1H, t, *J*=5.5, 4.8 Hz, H-6), 3.59 (1H, s, OH-5), 3.76 (1H, tq, *J*= 10.4, 5.0 Hz, H-3), 4.22 (1H, d, *J*=5.6 Hz, OH-3), 4.49 (1H, d, *J*=5.5 Hz, OH-6), 5.08 (1H, dt, *J*=4.8, 2.2 Hz, H-7), 5.17 (1H, dd, *J*=15.3, 8.3 Hz, H-22), 5.25 (1H, dd, *J*=15.3, 7.4 Hz, H-23); ^{13}C-NMR (DMSO-d_6, 151 MHz) δ 12.1 (C-18), 17.2 (C-28), 17.7 (C-19), 19.5 (C-26), 19.8 (C-27), 20.9 (C-21), 21.3 (C-16), 22.5 (C-15), 27.6 (C-11), 31.1 (C-2), 32.4 (C-1, C-25), 36.6 (C-10), 38.9 (C-12), 39.9 (C-20), 40.1 (C-4), 42.0 (C-24), 42.2 (C-9), 42.9 (C-13), 54.1 (C-14), 55.3 (C-17), 65.9 (C-3), 72.1 (C-6), 74.4 (C-5), 119.5 (C-7), 131.4 (C-23), 138.4 (C-22), 139.6 (C-8). HRMS/MS *m/z* 453.3397 $[M + Na]^+$, calcd for $C_{28}H_{46}O_3Na$ 453.3345.

6-Dehydrocerevisterol (**21**): White amorphous solid (0.6 mg); ^{1}H-NMR (DMSO-d_6, 600 MHz) δ 0.55 (3H, s, H_3-18), 0.78 (3H, s, H_3-19), 0.81 (3H, d, *J*=7.0 Hz, H_3-27), 0.80 (3H, d, *J*=7.0 Hz, H_3-26), 0.89 (3H, d, *J*=6.8 Hz, H_3-28), 1.00 (3H, d, *J*=6.6 Hz, H_3-21), 3.71 (1H, tq, *J*= 7.0, 5.5 Hz, H-3), 4.40 (1H, d, *J*=5.5 Hz, OH-3), 5.12 (1H, s, OH-5), 5.18 (1H, dd, *J*=15.3, 8.4 Hz, H-22), 5.25 (1H, dd, *J*=15.3, 7.4 Hz, H-23), 5.39 (1H, t, *J*=2.4 Hz, H-7); ^{13}C-NMR (DMSO-d_6, 151 MHz) δ 12.4 (C-18), 15.8 (C-19), 17.3 (C-28), 19.5 (C-27), 19.7 (C-26), 20.9 (C-21), 21.2 (C-11), 22.0 (C-15), 27.6 (C-16), 30.0 (C-1), 30.4 (C-2), 32.5 (C-25), 35.9 (C-4), 38.1 (C-12), 39.8 (C-20), 40.1 (C-10), 42.0 (C-24), 43.2 (C-9), 44.0 (C-13), 54.8 (C-14), 55.2 (C-17), 65.5 (C-3), 76.0 (C-5), 119.3 (C-7), 131.6 (C-23), 135.1 (C-22), 163.3 (C-8), 198.6 (C-6). HRMS/MS *m/z* 429.3387 $[M + H]^+$, calcd for $C_{28}H_{45}O_3$, 429.3368.

Ergosterol (**22**): White amorphous solid (0.4 mg); ^{1}H-NMR (DMSO-d_6, 600 MHz) δ 0.59 (3H, s, H_3-18), 0.80 (3H, d, *J*=6.9 Hz, H_3-27), 0.81 (3H, d, *J*=7.0 Hz, H_3-26), 0.86 (3H, s, H_3-19), 0.89 (3H, d, *J*=6.8 Hz, H_3-28), 1.01 (3H, d, *J*=6.6 Hz, H_3-21), 3.36 (1H, overlapped, H-3), 4.40 (1H, d, *J*=4.4 Hz, OH-3), 5.18 (1H, dd, *J*=15.3, 8.1 Hz, H-22), 5.24 (1H, dd, *J*=15.3, 7.2 Hz, H-23), 5.32 (1H, dt, *J*=5.0. 2.1 Hz, H-7), 5.47 (1H, dd *J*=5.5. 2.1 Hz, H-7); ^{13}C-NMR (DMSO-d_6, 151 MHz) δ 11.8 (C-18), 16.0 (C-19), 17.3 (C-28), 19.5 (C-26), 19.8 (C-27), 20.6 (C-11), 21.0 (C-21), 22.6 (C-15), 27.9 (C-16), 31.8 (C-2), 32.5 (C-25), 36.6 (C-10), 37.9 (C-1), 38.4 (C-12), 39.9 (C-20), 40.7 (C-4), 42.0 (C-24), 42.3 (C-13), 45.7 (C-9), 53.9 (C-14), 55.0 (C-17), 68.6 (C-3), 116.2 (C-7), 118.7 (C-6), 131.4 (C-23), 135.4 (C-22), 140.2 (C-8), 140.6 (C-5). HRMS/MS *m/z* 395.3325 $[M - H]^-$, calcd for $C_{28}H_{45}O$, 395.3313.

4.10 Minimum inhibitory concentration test

Methicillin-resistant *Staphylococcus aureus* (MRSA, ATCC 33591) and *Pseudomonas aeruginosa* (ATCC 27853) strains were used for the antibacterial assay. The minimum inhibitory concentration (MIC) of the extract and the isolated compounds were determined in triplicates according to Wiegand et al. (2008) in Mueller-Hinton medium (MH). After the incubation of the inoculated 96-well plates at 37°C for 24h, iodonitrotetrazolium chloride (INT, Sigma-Aldrich) was added to each well at a final concentration of 0.2 mg/mL and incubated for 20 minutes) (Eloff, 1998). The highest dilution of a compound in which no growth appears corresponds to its MIC. Gentamicin for *P. aeruginosa* and chloramphenicol for *S. aureus* were used as controls.

4.11 Anti-quorum sensing assay for *Pseudomonas aeruginosa*

The assay was performed according to the protocol proposed by Hentzer et al. (2002) on a black 96 well plate with clear bottom. Reporter strain PPAO1 *pqsA::gfp*, was constructed using the following primers GCTCTAGATCGAGCAAGGGTTGTAACGGTTTTTG and GCTGCTGCATGCGACAGAACGTTCCCTCTTCAGCGA to amplify *pqsA* gene promoter and cloned by usual molecular methods into XbaI-SphI sites of *lasB::gfp* plasmid (Hentzer et al., 2002), in place of the *lasB* promoter. Reporter strains containing the *lasB::gfp* or the *pqsA::gfp* plasmid were grown at starting OD600 of 0.05 in PTSB (5% peptone, 0.25% trypticase soy broth) supplied with gentamicin 50 µg/ml and each sample at 128 µg/ml. Azithromycin 2 µg/ml was used as positive control. Plates were incubated at 37°C, 160 rpm. After 15 hours, OD600 and fluorescence at 480/520 nm were measured using a microplate reader (SynergyHT BioTek). Results are represented in percentage of fluorescence compared to the solvent control (DMSO) fixed at 100%.

4.12 Anti-quorum sensing assay for *Staphylococcus aureus*

The assay was performed according to the protocol proposed by Nielsen et al. (2010). In a 96 well plate, the reporter strain *rnaIII::lacZ* (Nielsen et al., 2010) was grown at a starting OD600 of 0.05 in MH, supplied with erythromycin 5 µg/ml and each sample at 128 µg/ml. *Staphylococcus caprae* autoinducing peptide (AIP) (Paharik et al., 2017) at concentration of 1 µM was used as positive control. After 6 hours at 37°C, 160 rpm, incubation was stopped and OD600 value was read. Then, 10 µl of freshly made 4-methylumbelliferyl-β-D-galactopyranoside (MUG) 10 mg/ml was added to each well and left to incubate for 1 hour at room temperature. Reaction was stopped by addition of 100 µl of Na_2CO_3 0.4M and fluorescence was read using a microplate reader (SynergyHT BioTek) at 360/460 nm. Results are represented in percentage of fluorescence compared to the solvent control (DMSO) fixed at 100%.

4.13 Quantitative qRT-PCR

Cultures were grown in triplicates during 4 hours in presence of the compound of interest at 128 µg/ml. Then, 1 ml of bacteria was treated with RNA protect Bacteria Reagent (Qiagen) before centrifugation and storage at -20°C. Pellets were resuspended in 100 µl TE pH8, 2.5 µl of lysostaphin 10 mg/ml for *S. aureus* PR01 and incubated 10 min. at 37°C, or 100 µl TE pH8, lysozyme 1 mg/ml and incubated 5 min. at RT for *P. aeruginosa* PAO1. RNA was extracted by RNeasy kit (Qiagen) according to the manufacturer's protocol. RNA was eluted in 40 µl of RNAse-free water, quantified using Qubit 2.0 fluorometer (invitrogen) and DNase treated with RQ1 RNase-free DNase (Promega) according to manufacturer's instructions. Then, 500 ng of RNA were reverse transcribed into cDNA using random primers (Promega) and Improm-II reverse transcriptase (Promega) according to the manufacturer. qPCR was performed using SYBR select master mix

(Thermo Fisher). Primers for the amplification of target genes are listed in Supplementary Table S4. *HU* and *oprF* genes were used for normalization for *S. aureus* and *P. aeruginosa*, respectively.

5 Abbreviations

^{1}H-NMR, Proton nuclear magnetic resonance; DMSO, dimethyl sulfoxide; F, fraction; FA, formic acid; GNPS, global natural products social molecular networking; LC-NMR, liquid Chromatography with Nuclear Magnetic Resonance Spectroscopy; *m/z*, mass to charge ratio; PQS, *Pseudomonas* quinolone signal; SPE, solid phase extraction; UHPLC-MS/MS, ultra-high performance liquid chromatography tandem mass spectrometry; UV, Ultra-violet; Z, chromatographic zones.

6 Acknowledgments

We would like to thank the BIO2MAR platform for their contribution to identify the fungal strains. Many thanks to Nina Lager-Lachaud and Nicole Lecoultre for initiating the primary cultivation and maintaining the strains. The authors are thankful to Yoan Ferandin for his contribution in plant collection and maintaining the *Fusarium* strains.

7 Data Availability Statement

The raw data of this work can be requested from the authors.

8 Author Contributions

JLW and EFQ supervised and designed the research. AA, LM, VH, KG, SL, and PMA conducted the experiments. AA, LM and VH analyzed the data and wrote the manuscript. EFQ, KP, DS, and JLW assisted the editing of the manuscript. All authors read and approved the manuscript.

9 Funding

This work has been granted by joint collaboration between Swiss National Science Foundation and Agence Nationale de la Recherche (SNSF-ANR) part of project SECIL (ref SNF N° 310030E-164289 and ANR-15-CE21-0016). JLW is thankful to the Swiss National Science Foundation for the support in the acquisition of the NMR 600 MHz (SNF Research Equipment grant 316030_164095). AA is thankful to the Saudi Ministry of Education and Saudi cultural mission in Paris for their kind financial and logistic support to his PhD thesis.

10 Conflict of Interest

The authors declare that the research was conducted in the absence of any commercial or financial relationships that could be construed as a potential conflict of interest.

11 Supplementary Materials

The Supplementary Materials for this article can be found online at:

991 **Figure Captions**

992 **Figure 1.** Schematic overview of the workflow of this study. **(A)** Optimized UHPLC-PDA-MS
993 profile of the ethyl acetate crude extract (base peak intensity (BPI), PI mode) and UV trace (254
994 nm). **(B)** HRMS/MS spectra of the LC peaks from the UHPLC-HRMS/MS extract profile
995 corresponding to the isolated compounds **9** and **10**. **(C)** Selected part of a molecular network cluster
996 highlighting the features of **9**, **10**, **16**, and **17** (series of structurally related pyrone derivatives).
997 Some of the other features were dereplicated based on MN annotation propagation see Table 2. **(D)**
998 HPLC-PDA chromatogram after gradient transfer from (A). Z1 to Z14 indicate chromatographic
999 zones combined in semi-preparative HPLC for the bioassay monitoring, shown on (D) for a clearer
1000 display. **(E)** semi-preparative HPLC-UV chromatogram after gradient transfer from (D) and dryload
1001 sample introduction; vertical lines represent collected fractions. **(F)** *Pseudo*-LC-NMR obtained by a
1002 combination of the ^{1}H-NMR spectra of all freations from (E) into a single matrix (ppm vs. RT or
1003 fraction Nº). **(G)** ^{1}H-NMR spectra of fractions F51 and F55 highlighted in the 2d plot (F).

1004 **Figure 2.** Most likely tree (-ln = 20922.71682) inferred from the *Fusarium* 5 locus-64 taxa dataset
1005 (alignment length after exclusion of ambiguously aligned regions = 2442 characters (char);
1006 calmodulin = 142 char, beta-tubulin = 262 char, ITS = 364 char, *RPB2* = 1500 char, TEF-1 = 174
1007 char). The fungal collection newly sequenced for that study is in blue. Branches that received
1008 significant bootstrap (BS) values (≥ 70%) are in bold with BS values reported along the branches.

1009 **Figure 3. (A)** Stacked view of the ^{1}H-NMR spectra of all fractions ordered by retention time from
1010 top to bottom, all recorded in DMSO-d_6 as bridging solvent. Green shadow highlights common
1011 signals in fractions F51-56 in the regions of δ_H 5.5 to 5.7, and δ_H 6.0 to 6.3. Orange shadow
1012 highlights common signals in fractions F64-65 and F103-104 in the region of δ_H 5.2 to 5.3. Yellow
1013 shadow highlights the presence of fatty acids. **(B)** UV trace of the semi-preparative HPLC
1014 chromatogram for LC peaks localization (Figure 1E). **(C)** Inset showing characteristic signals of the
1015 series across a set of fractions F51-56 and 90-93. **(D)** Inset showing characteristic signals of the
1016 series across a set of fractions F64-65 and 103-104.

1017 **Figure 4.** Structures of isolated compounds **1**-**22**.

1018 **Figure 5. (A)** Structure of **12**. **(B)** ROESY NMR spectrum of **12** in DMSO-d_6 **(C)** Observed
1019 ROESY correlations for compound **12**.

1020 **Figure 6.** HPLC-PDA-ELSD analysis highlighting the effect of the extract enrichment and location
1021 of various bioactivities monitoring. **(A)** Chromatogram of the crude extract, dashed lines represent
1022 the 14 chromatographic zones. Highlighted zones represent the part of the chromatogram for
1023 possible bioactivity. The square in the ELSD highlights the presence of fatty acids. **(B)**
1024 chromatogram of the hydroalcoholic part. **(C)** chromatogram of the hexane. Compounds that
1025 possess bioactivity are annotated by colored circles and the process demonstrates that they can be
1026 precisely localized after enrichment.

1027 **Figure 7. (A)** Quantitative PCR test of *S. aureus* QS regulated genes *hla* and *hld*. AIP (autoinducer
1028 from *S. caprae*) is used as positive inhibitor control **(B)** Quantitative PCR test of *P. aeruginosa* for
1029 QS regulated gene *pqsA*. Fold induction is represented relative to DMSO alone (fixed at 1).

1030

1031 **Table 1.** Minimum Inhibitory Concentration (MIC) and quorum sensing inhibition (QS) assays of
1032 crude extract compared to several antibiotics.

1033

	MIC (µg/ml)		QS (% of fluorescence)	
	MRSA	PA	PA (*pqsA*)	PA (*lasB*)
Crude extract (small scale)	32	> 128	21%	19%
Crude extract (large scale)	32	> 128	20%	25%
Azithromycin	NA	10	32%	39%
Gentamicin	1	NA		
Tetracycline	16			
Erythromycin	16			
Chloramphenicol	32			

Values show the mean of triplicates. Test results were compared to DMSO fixed at 100%. MRSA, methicillin resistant Staphylococcus aureus; PA, Pseudomonas aeruginosa; NA, not applicable.

1034

Table 2. Annotated compounds by UHPLC-HRMS/MS in both PI and NI modes in the crude extract of *F. petroliphilum*.

N° F.	N° C.	RT	C. Index	Isolated as	Annotated as	T. score	Chemical class	MF	I. mode	*m/z*	Error (ppm)
F4	1	1.03	Sgl	Adenosine	Adenosine	3	Purine Nucleoside	$C_{10}H_{13}N_5O_4$	$[M+H]^+$	268.1039	-1.49
F10	3	2.31	19	6-(1-hydroxyethyl)-3-methyl-2H-pyran-2-one	-	3	Pyrone	$C_8H_{10}O_3$	$[M+H]^+$	155.0703	-3.22
F10	2a	2.21	155	6-(2,3-dihydroxybutan-2-yl)-3-methyl-2H-pyran-2-one	Fusanolide B	3	Pyrone	$C_{10}H_{14}O_4$	$[M+H]^+$	199.0967	-2.51
F10	2b	2.27	155	Isomer of 2a	Fusanolide B	3	Pyrone	$C_{10}H_{14}O_4$	$[M+H]^+$	199.0872	-1.51
-	-	2.45	3	-	Arthropsolide A	2	Polyketide	$C_{13}H_{14}O_5$	$[M-H]^-$	249.0766	-1.2
-	-	2.47	145	-	Fusaquinone A	2	Naphthofuran	$C_{16}H_{18}O_6$	$[M+H]^+$	307.1178	-1.17

-	-	2.56	145	-	Fusarnaphthoquinone B	2	Naphthofuran	$C_{15}H_{16}O_5$	$[M+H]^+$	277.1066	-3.61
-	-	2.59	9	-	Diaporthin	1	Benzopyone	$C_{13}H_{14}O_5$	$[M+H]^+$	251.0911	-3.65
F20	4	2.65	329	Gibepyrone D	Gibepyrone D	2	Pyrone	$C_{10}H_{10}O_4$	$[M-H]^-$	193.0498	-1.55
F26	5	2.71	37	Aloesol	Aloesol	2	Benzopyran	$C_{13}H_{14}O_4$	$[M+H]^+$	235.0963	-2.97
			Sgl						$[M-H]^-$	233.0821	3.42
-	-	2.74	Sgl	-	Cladobotrin V	2	Pyranone	$C_{10}H_{12}O_4$	$[M-H]^-$	195.0655	-0.85
-	-	2.95	222	-	Javanicin O-De-Me	2	Naphthoquinone	$C_{14}H_{12}O_6$	$[M-H]^-$	275.0564	3.08
-	-	3.01	Sgl	-	Gibepyrone A	3	Pyranone	$C_{10}H_{12}O_2$	$[M-H]^-$	163.0753	-0.22
-	-	3.2	19	-	Fusarpyrone A	3	Pyran	$C_{10}H_{12}O_3$	$[M+H]^+$	181.0858	0.8

-	-	3.23	222	-	5,8-Dihydroxy-6-hydroxymethyl-7-(2-hydroxypropyl)-2-methoxy-1,4-naphthoquinone	3	Naphthoquinone	$C_{15}H_{15}O_7$	$[M-H]^-$	307.0825	2.44
-	-	3.24	9	-	Fusarubin 5-deoxy	3	Benzoquinone	$C_{15}H_{14}O_6$	$[M+H]^+$	291.086	-2.8
-	-	3.37	207	-	Bostrycoidin 6-Deoxy	3	Quinone	$C_{15}H_{11}NO_4$	$[M+H]^+$	270.0759	-2.76
F35	6	6.63	207	5-hydroxy-4-(hydroxymethyl)-8-methoxy-2-methyl-1H-benzo[g]indole-6,9-dione	-	3	Quinone	$C_{15}H_{13}NO_5$	$[M+H]^+$	288.0868	-1.38
-	-	3.37	5	-	Sescandelin 1'-Ketone	1	Isocoumarin	$C_{11}H_8O_5$	$[M-H]^-$	219.0295	1.6
-	-	3.85	306	-	5-Acetyl-1,2,4,6-tetrahydroxyanthraquinone2-Me ether	2	Quinone	$C_{17}H_{12}O_7$	$[M+H]^+$	329.0636	2.6
F43	7	3.86	9	Fusarubin	Fusarubin	3	Benzoquinone	$C_{15}H_{14}O_7$	$[M+H]^+$	307.0823	1.62

F44	8	3.86	-	3-O-Methylfusarubin	3-O-Methylfusarubin	3	Quinone	$C_{16}H_{16}O_7$	$[M-H]^-$	319.0825	2.19
-	-	3.86	45	-	Anhydrofusarubin	3	Quinone	$C_{15}H_{12}O_6$	$[M+H]^+$	289.0715	1.03
-	-	3.87	54	-	3-Acetonyl-2,5,8-trihydroxy-6-methoxy naphthoquinone	3	Naphthoquinone	$C_{14}H_{12}O_7$	$[M-H]^-$	291.0511	1.04
F51	9	3.96	25	(6E)-7-(4-methoxy-6-oxo-6H-pyran-2-yl)-3,5-dimethyloct-6-enoic acid	7S-Hydroxy-O-demethyllasiodiplodin	3	Pyran	$C_{16}H_{22}O_5$	$[M+H]^+$	295.1544	-3.72
-	x	3.97	54	-	Rhodolamprometrin	2	Anthracene	$C_{16}H_{10}O_7$	$[M-H]^-$	313.0352	1.13
F55	10	4.4	29	6-((E)-6-ethyl-7-hydroxy-4-methylhept-2-en-2-yl)-4-methoxy-2H-pyran-2-one	-	3	Pyrone	$C_{16}H_{24}O_4$	$[M+H]^+$	281.1745	-2.13
-	-	4.54	45	-	Solaniol or Karuquinone C	3	Naphthalene	$C_{15}H_{16}O_6$	$[M+H]^+$	293.1017	-2.73
		4.55	54						$[M-H]^-$	291.0885	4.8

-	-	4.61	45	-	Dihydroanhydrojavanicin	3	Naphthofuran	$C_{15}H_{14}O_5$	$[M+H]^+$	275.0912	-1.89
F60	11	5.63	19	Bostrycoidin	Bostrycoidin	3	Quinone	$C_{15}H_{11}NO_5$	$[M+H]^+$	286.0695	-0.34
F62	12	5.34	Sgl	5β,6β-23,26-diepoxy-3β,7α,9α-trihydroxy-(20Z,23S,24S,25R)ergosta-8(14),20-dien-15-one	-	3	Steroid	$C_{28}H_{40}O_6$	$[M+Na]^+$	495.2706	-3.23
F64	13	5.44	86	2-(2,3,5,6,7,7a-hexahydro-1-((E)-6-hydroxy-5,6-dimethylhept-3-en-2-yl)-7a-methyl-5-oxo-1H-inden-4-yl)acetic acid	-	3	Cyclohexenone	$C_{21}H_{32}O_4$	$[M+H]^+$	349.2378	-0.28
		5.44	Sgl						$[M-H]^-$	347.2228	1.72
F66	14	5.68	86	2-(2,3,5,6,7,7a-hexahydro-1-((E)-7-hydroxy-5,6-dimethylhept-3-en-2-yl)-7a-methyl-5-oxo-1H-inden-4-yl)acetic acid	-	3	Cyclohexenone	$C_{21}H_{32}O_4$	$[M+H]^+$	349.2386	2
			Sgl						$[M-H]^-$	347.2232	2.87

F69	15	3.38	Sgl	5-hydroxy-4-methoxy-6,8-dimethylpyrano[3,2-g]indol-2(9H)-one	-	3	Pyrone	$C_{14}H_{13}NO_4$	$[M-H]^-$	258.0771	1.82
-	-	7.05	173	-	kauranoic acid ent-16β-Hydroxy-19	2	Fatty acid	$C_{20}H_{32}O_3$	$[M+H]^+$	321.2442	2.1
-	-	7.81	19	-	Fusarone	2	Cyclopentanone	$C_{14}H_{22}O_3$	$[M+H]^+$	239.1661	0.5
F91	16	8.89	29	4-methoxy-6-((E)-4,6-dimethyloct-2-en-2-yl)-2H-pyran-2-one	-	3	Pyrone	$C_{16}H_{24}O_3$	$[M+H]^+$	265.1805	0.37
F93	17	9.6	Sgl	4-methoxy-3-methyl-6-((E)-4,6-dimethyloct-2-en-2-yl)-2H-pyran-2-one	-	3	Pyrone	$C_{17}H_{26}O_3$	$[M+H]^+$	279.1956	-1.43
F103	18	11.34	Sgl	2-(2,3,5,6,7,7a-hexahydro-7a-methyl-1-((E)-5,6-dimethylhept-3-en-2-yl)-5-oxo-1H-inden-4-yl)acetic acid	-	3	Cyclohexenone	$C_{21}H_{32}O_3$	$[M+H]^+$	333.2426	0.3
									$[M-H]^-$	331.228	2.11

107	19	14.5	-	3-O-β-D-glucopyranoside-Stigmast-8-en-3-ol	-	3	Steroid	$C_{35}H_{60}O_6$	$[M+Na]^+$	599.428	-1.16
F116	20	14.6	-	24R/24S Cerevisterol	-	3	Steroid	$C_{28}H_{46}O_3$	$[M+Na]^+$	453.3397	11.6
F117	21	14.27	-	6-Dehydrocerevisterol	-	3	Steroid	$C_{28}H_{44}O_3$	$[M+H]^+$	429.3387	4.42
F122	x	16.48	-	-	3-Acetoxy-2,3-dihydropiptoporic acid	1	Fatty acid	$C_{23}H_{28}O_5$	$[M-H]^-$	383.1898	1.8
F132	22	13.62	-	Ergosterol	Ergosterol	3	Steroid	$C_{28}H_{44}O$	$[M-H]^-$	395.3325	2.78

*N° F., = Number of semi-preparative fraction; N° C. = Isolated compounds **1**–**22**; RT = retention time in UHPLC-HRMS/MS analysis of the extract; C. index = component index (cluster number in MN); Sgl = singleton node; T. score = taxonomically informed score; I.mode = ionization mode; 1 = family (Nectriaceae); 2 = genus (Fusarium); 3 = species (F. solani); MF = molecular formula.*

Table 3. Minimum Inhibitory Concentration (MIC) and quorum sensing inhibition (QS) assays of zones of fractions and their corresponding compounds compared to several positive controls.

Zone	% PA (*pqsA*)	% PA (*lasB*)	Compound	% PA (*pqsA*)	% PA (*lasB*)	% SA (*lacZ*)
Control	32 ± 0.2	39 ± 2.9	NA	32 ± 0.2	39 ± 2.9	27 ± 1.6
Z_3	68 ± 0.0	85 ± 0.2	(**4**)	60 ± 4.5	76 ± 8.0	79 ± 0.7
			(**5**)	40 ± 8.5	51 ± 7.7	**11** ± 5.0
Z_4	48 ± 2.6	65 ± 1.2	(**6**)	59 ± 2.7	69 ± 0.9	37 ± 0.0
Z_5	31 ± 1.6	43 ± 0.4	(**7**/**8**)	**12** ± 0.6	**15** ± 1.0	**3** ± 0.5*
Z_6	45 ± 0.7	60 ± 0.9	(**9**)	58 ± 3.6	68 ± 2.7	90 ± 0.0
			(**10**)	36 ± 2.2	41 ± 0.4	**17** ± 4.2
Z_7	60 ± 4.3	75 ± 0.4	(**11**)	66 ± 10.1	71 ± 0.5	121 ± 22.0
			(**12**)	58 ± 3.6	68 ± 2.7	79 ± 0.7
			(**13**)	34 ± 2.6	**39** ± 0.4	**13** ± 0.2
Z_8	64 ± 0.3	82 ± 1.8	(1**4**)	72 ± 6.5	73 ± 0.2	31 ± 1.2

			(**15**)	57 ± 2.9	63 ± 0.1	36 ± 3.3
Z_9 (MIC MRSA at 32 µg/ml)	63 ± 0.6	82 ± 0.0	(**16**) (MIC MRSA at 32 µg/ml)	37 ± 2.1	39 ± 6.9	**15** ± 11.0

*Values show the mean of triplicates ± SD. Values in **bold** are lower than the corresponding control. Positive controls of QS assays are, azithromycin at 2 µg/ml for PA, and S. caprae AIP 1 µM for SA. Results were compared to DMSO fixed at 100%. MRSA, methicillin resistant Staphylococcus aureus; PA, Pseudomonas aeruginosa; NA, not applicable. *Fluorescence was biased due to the natural coloration of the compound.*

12 References

Alfaro, M.E., Zoller, S., and Lutzoni, F. (2003). Bayes or bootstrap? A simulation study comparing the performance of Bayesian Markov chain Monte Carlo sampling and bootstrapping in assessing phylogenetic confidence. *Mol. Biol. Evol.* 20(2)**,** 255-266. doi: 10.1093/molbev/msg028.

Allard, P.M., Peresse, T., Bisson, J., Gindro, K., Marcourt, L., Pham, V.C., et al. (2016). Integration of molecular networking and *in-Silico* MS/MS fragmentation for natural products dereplication. *Anal. Chem.* 88(6)**,** 3317-3323. doi: 10.1021/acs.analchem.5b04804.

Arsenault, G.P. (1965). The structure of bostrycoidin, a β-aza-anthraquinone from *Fusarium solani* D2 purple. *Tetrahedron Lett.* 6(45)**,** 4033-4037. doi: 10.1016/S0040-4039(01)99610-8.

Ayer, W.A., Craw, P.A., and Neary, J. (1992). Metabolites of the fungus Arthropsistruncata. *Can. J. Chem.* 70(5)**,** 1338-1347. doi: 10.1139/v92-172.

Bassler, B.L., and Losick, R. (2006). Bacterially speaking. *Cell* 125(2)**,** 237-246. doi: 10.1016/j.cell.2006.04.001.

Blunt, J.W., Carroll, A.R., Copp, B.R., Davis, R.A., Keyzers, R.A., and Prinsep, M.R. (2018). Marine natural products. *Nat. Prod. Rep.* 35(1)**,** 8-53. doi: 10.1039/c7np00052a.

Bohni, N., Hofstetter, V., Gindro, K., Buyck, B., Schumpp, O., Bertrand, S., et al. (2016). Production of fusaric acid by *Fusarium spp.* in pure culture and in solid medium co-cultures. *Molecules* 21(3)**,** 370. doi: 10.3390/molecules21030370.

Brown, E.D., and Wright, G.D. (2016). Antibacterial drug discovery in the resistance era. *Nature* 529(7586)**,** 336-343. doi: 10.1038/nature17042.

Carbone, I., and Kohn, L.M. (2019). A method for designing primer sets for speciation studies in filamentous ascomycetes. *Mycologia* 91(3)**,** 553-556. doi: 10.1080/00275514.1999.12061051.

Cardoso, J., Thomasi, S., Venâncio, T., Pitta, I., de Lima, M.d.C., and Oliveira, R. (2016). Preparative separation and structural identification of impurities of a new α_2- adrenoceptor agonist using stacking injection, LC-MS^n and LC-SPE-NMR. *J. Braz. Chem. Soc.* 28(6)**,** 1038-1047. doi: 10.21577/0103-5053.20160259.

Chang, C.C., Tsai, W.T., Chen, C.K., Chen, C.H., and Lee, S.S. (2020). Diastereomeric identification of neolignan rhamnosides from Trochodendron aralioides leaves by LC-SPE-NMR and circular dichroism. *Fitoterapia* 144**,** 7. doi: 10.1016/j.fitote.2019.104455.

Chehri, K., Salleh, B., and Zakaria, L. (2015). Morphological and phylogenetic analysis of *Fusarium solani* species complex in Malaysia. *Microb. Ecol.* 69(3)**,** 457-471. doi: 10.1007/s00248-014-0494-2.

Church, D., Elsayed, S., Reid, O., Winston, B., and Lindsay, R. (2006). Burn wound infections. *Clin. Microbiol. Rev.* 19(2)**,** 403-434. doi: 10.1128/CMR.19.2.403-434.2006.

Ciuffreda, P., Casati, S., and Manzocchi, A. (2007). Complete (1)H and (13)C NMR spectral assignment of alpha- and beta-adenosine, 2'-deoxyadenosine and their acetate derivatives. *Magn. Reson. Chem.* 45(9)**,** 781-784. doi: 10.1002/mrc.2036.

Cordell, G.A. (2000). Biodiversity and drug discovery — a symbiotic relationship. *Phytochemistry* 55(6)**,** 463-480. doi: 10.1016/s0031-9422(00)00230-2.

Dias, D.A., and Urban, S. (2009). Application of HPLC-NMR for the rapid chemical profiling of a Southern Australian sponge, *Dactylospongia sp*. *J. Sep. Sci.* 32(4)**,** 542-548. doi: 10.1002/jssc.200800548.

Eloff, J.N. (1998). A sensitive and quick microplate method to determine the minimal inhibitory concentration of plant extracts for bacteria. *Planta Med.* 64(8)**,** 711-713. doi: 10.1055/s-2006-957563.

Exarchou, V., Krucker, M., van Beek, T.A., Vervoort, J., Gerothanassis, I.P., and Albert, K. (2005). LC-NMR coupling technology: recent advancements and applications in natural products analysis. *Magn. Reson. Chem.* 43(9)**,** 681-687. doi: 10.1002/mrc.1632.

Foster, T.J., Geoghegan, J.A., Ganesh, V.K., and Hook, M. (2014). Adhesion, invasion and evasion: the many functions of the surface proteins of *Staphylococcus aureus*. *Nat. Rev. Microbiol.* 12(1)**,** 49-62. doi: 10.1038/nrmicro3161.

Gad, M., Tuenter, E., El-Sawi, N., Younes, S., El-Ghadban, E.M., Demeyer, K., et al. (2018). Identification of some bioactive metabolites in a fractionated methanol extract from ipomoea aquatica (aerial parts) through TLC, HPLC, UPLC-ESI-QTOF-MS and LC-SPE-NMR fingerprints analyses. *Phytochem. Anal.* 29(1)**,** 5-15. doi: 10.1002/pca.2709.

Glass, N.L., and Donaldson, G.C. (1995). Development of primer sets designed for use with the PCR to amplify conserved genes from filamentous ascomycetes. *Appl. Environ. Microbiol.* 61(4)**,** 1323-1330. doi: 10.1128/aem.61.4.1323-1330.1995.

Guillarme, D., Nguyen, D.T., Rudaz, S., and Veuthey, J.L. (2008). Method transfer for fast liquid chromatography in pharmaceutical analysis: application to short columns packed with small particle. Part II: gradient experiments. *Eur. J. Pharm. Biopharm.* 68(2)**,** 430-440. doi: 10.1016/j.ejpb.2007.06.018.

Guindon, S., and Gascuel, O. (2003). A simple, fast, and accurate algorithm to estimate large phylogenies by maximum likelihood. *Syst. Biol.* 52(5)**,** 696-704. doi: 10.1080/10635150390235520.

Hammerl, R., Frank, O., Schmittnagel, T., Ehrmann, M.A., and Hofmann, T. (2019). Functional metabolome analysis of *penicillium roqueforti* by means of differential off-line LC-NMR. *J. Agric. Food Chem.* 67(18)**,** 5135-5146. doi: 10.1021/acs.jafc.9b00388.

Hentzer, M., Riedel, K., Rasmussen, T.B., Heydorn, A., Andersen, J.B., Parsek, M.R., et al. (2002). Inhibition of quorum sensing in *Pseudomonas aeruginosa* biofilm bacteria by a halogenated furanone compound. *Microbiology (Reading)* 148(Pt 1)**,** 87-102. doi: 10.1099/00221287-148-1-87.

Hernando-Amado, S., Coque, T.M., Baquero, F., and Martínez, J.L. (2019). Defining and combating antibiotic resistance from One Health and Global Health perspectives. *Nature Microbiology* 4(9)**,** 1432-1442. doi: 10.1038/s41564-019-0503-9.

Hofstetter, V., Clémençon, H., Vilgalys, R., and Moncalvo, J.-M. (2002). Phylogenetic analyses of the Lyophylleae (Agaricales, Basidiomycota) based on nuclear and mitochondrial rDNA sequences. *Mycol. Res.* 106(9)**,** 1043-1059. doi: 10.1017/s095375620200641x.

Holden, M.T., Hsu, L.Y., Kurt, K., Weinert, L.A., Mather, A.E., Harris, S.R., et al. (2013). A genomic portrait of the emergence, evolution, and global spread of a methicillin-resistant

Staphylococcus aureus pandemic. *Genome Res.* 23(4)**,** 653-664. doi: 10.1101/gr.147710.112.

Hou, R., Jiang, C., Zheng, Q., Wang, C., and Xu, J.-R. (2015). The AreA transcription factor mediates the regulation of deoxynivalenol (DON) synthesis by ammonium and cyclic adenosine monophosphate (cAMP) signalling in *Fusarium graminearum*. *Mol. Plant Pathol.* 16(9)**,** 987-999. doi: 10.1111/mpp.12254.

Jimenez, P.N., Koch, G., Thompson, J.A., Xavier, K.B., Cool, R.H., and Quax, W.J. (2012). The multiple signaling systems regulating virulence in *Pseudomonas aeruginosa*. *Microbiol. Mol. Biol. Rev.* 76(1)**,** 46-65. doi: 10.1128/MMBR.05007-11.

Kashiwada, Y., Nonaka, G., and Nishioka, I. (1984). Studies on rhubarb (rhei rhizoma). V. Isolation and characterization of chromone and chromanone derivatives. *Chem. Pharm. Bull.* 32(9)**,** 3493-3500. doi: 10.1248/cpb.32.3493.

Kawagishi, H., Katsumi, R., Sazawa, T., Mizuno, T., Hagiwara, T., and Nakamura, T. (1988). Cytotoxic steroids from the mushroom *Agaricus blazei*. *Phytochemistry* 27(9)**,** 2777-2779. doi: 10.1016/0031-9422(88)80662-9.

Kour, A., Shawl, A.S., Rehman, S., Sultan, P., Qazi, P.H., Suden, P., et al. (2007). Isolation and identification of an endophytic strain of *Fusarium oxysporum* producing podophyllotoxin from *Juniperus recurva*. *World J. Microbiol. Biotechnol.* 24(7)**,** 1115-1121. doi: 10.1007/s11274-007-9582-5.

Kwon, H.C., Zee, S.D., Cho, S.Y., Choi, S.U., and Lee, K.R. (2002). Cytotoxic ergosterols from *Paecilomyces sp.* J300. *Arch. Pharm. Res.* 25(6)**,** 851-855. doi: 10.1007/BF02977003.

Liu, Y.J., Whelen, S., and Hall, B.D. (1999). Phylogenetic relationships among ascomycetes: evidence from an RNA polymerse II subunit. *Mol. Biol. Evol.* 16(12)**,** 1799-1808. doi: 10.1093/oxfordjournals.molbev.a026092.

Maddison, W.P., and Maddison, D.R. (1989). Interactive analysis of phylogeny and character evolution using the computer program MacClade. *Folia Primatol. (Basel)* 53(1-4)**,** 190-202. doi: 10.1159/000156416.

Morehouse, E.A., James, T.Y., Ganley, A.R., Vilgalys, R., Berger, L., Murphy, P.J., et al. (2003). Multilocus sequence typing suggests the chytrid pathogen of amphibians is a recently emerged clone. *Mol. Ecol.* 12(2)**,** 395-403. doi: 10.1046/j.1365-294x.2003.01732.x.

Newman, D.J., and Cragg, G.M. (2020). Natural products as sources of new drugs over the nearly four decades from 01/1981 to 09/2019. *J. Nat. Prod.* 83(3)**,** 770-803. doi: 10.1021/acs.jnatprod.9b01285.

Ng, W.L., and Bassler, B.L. (2009). Bacterial quorum-sensing network architectures. *Annu. Rev. Genet.* 43**,** 197-222. doi: 10.1146/annurev-genet-102108-134304.

Nielsen, A., Nielsen, K.F., Frees, D., Larsen, T.O., and Ingmer, H. (2010). Method for screening compounds that influence virulence gene expression in *Staphylococcus aureus*. *Antimicrob. Agents Chemother.* 54(1)**,** 509-512. doi: 10.1128/AAC.00940-09.

Nisa, H., Kamili, A.N., Nawchoo, I.A., Shafi, S., Shameem, N., and Bandh, S.A. (2015). Fungal endophytes as prolific source of phytochemicals and other bioactive natural products: A review. *Microb. Pathog.* 82**,** 50-59. doi: 10.1016/j.micpath.2015.04.001.

Niu, S., Tang, X.-X., Fan, Z., Xia, J.-M., Xie, C.-L., and Yang, X.-W. (2019). Fusarisolins A–E, Polyketides from the Marine-Derived Fungus *Fusarium solani* H918. *Mar. Drugs* 17(2)**,** 125. doi: 10.3390/md17020125.

Nothias, L.-F., Petras, D., Schmid, R., Dührkop, K., Rainer, J., Sarvepalli, A., et al. (2020). Feature-based molecular networking in the GNPS analysis environment. *Nat. Methods* 17(9)**,** 905-908. doi: 10.1038/s41592-020-0933-6.

O'Donnell, K. (2019). Molecular phylogeny of the *Nectria haematococca-Fusarium solani* species complex. *Mycologia* 92(5)**,** 919-938. doi: 10.1080/00275514.2000.12061237.

Paharik, A.E., Parlet, C.P., Chung, N., Todd, D.A., Rodriguez, E.I., Van Dyke, M.J., et al. (2017). Coagulase-Negative Staphylococcal Strain Prevents *Staphylococcus aureus* Colonization and Skin Infection by Blocking Quorum Sensing. *Cell Host Microbe* 22(6)**,** 746-756 e745. doi: 10.1016/j.chom.2017.11.001.

Paytubi, S., de La Cruz, M., Tormo, J.R., Martín, J., González, I., González-Menendez, V., et al. (2017). A high-throughput screening platform of microbial natural products for the discovery of molecules with antibiofilm properties against *Salmonella*. *Front. Microbiol.* 8(326). doi: 10.3389/fmicb.2017.00326.

Peric-Concha, N., and Long, P.F. (2003). Mining the microbial metabolome: a new frontier for natural product lead discovery. *Drug Discov. Today* 8(23)**,** 1078-1084. doi: 10.1016/s1359-6446(03)02901-5.

Pluskal, T., Castillo, S., Villar-Briones, A., and Oresic, M. (2010). MZmine 2: modular framework for processing, visualizing, and analyzing mass spectrometry-based molecular profile data. *BMC Bioinformatics* 11**,** 395. doi: 10.1186/1471-2105-11-395.

Qiao, M.-F., Yi, Y.-W., and Deng, J. (2017). Steroids from an endophytic *Eurotium rubrum* strain. *Chem. Nat. Compd.* 53(4)**,** 678-681. doi: 10.1007/s10600-017-2089-x.

Queiroz, E.F., Alfattani, A., Afzan, A., Marcourt, L., Guillarme, D., and Wolfender, J.-L. (2019). Utility of dry load injection for an efficient natural products isolation at the semi-preparative chromatographic scale. *J. Chromatogr.* 1598**,** 85-91. doi: 10.1016/j.chroma.2019.03.042.

Queiroz, E.F., Wolfender, J.L., Atindehou, K.K., Traore, D., and Hostettmann, K. (2002). On-line identification of the antifungal constituents of Erythrina vogelii by liquid chromatography with tandem mass spectrometry, ultraviolet absorbance detection and nuclear magnetic resonance spectrometry combined with liquid chromatographic micro-fractionation. *J. Chromatogr. A* 974(1-2)**,** 123-134. doi: 10.1016/s0021-9673(02)01224-4.

Richard, T., Temsamani, H., Cantos-Villar, E., and Monti, J.-P. (2013). "Application of LC–MS and LC–NMR techniques for secondary metabolite identification," in *Metabolomics Coming of Age with its Technological Diversity,* ed. D. Rolin. (San Diego: Elsevier Academic Press Inc), 67-98.

Rutz, A., Dounoue-Kubo, M., Ollivier, S., Bisson, J., Bagheri, M., Saesong, T., et al. (2019). Taxonomically informed scoring enhances confidence in natural products annotation. *Front Plant Sci* 10(1329)**,** 1329. doi: 10.3389/fpls.2019.01329.

Saeki, E.K., Kobayashi, R.K.T., and Nakazato, G. (2020). Quorum sensing system: Target to control the spread of bacterial infections. *Microb. Pathog.* 142**,** 104068. doi: 10.1016/j.micpath.2020.104068.

Schoch, C.L., Seifert, K.A., Huhndorf, S., Robert, V., Spouge, J.L., Levesque, C.A., et al. (2012). Nuclear ribosomal internal transcribed spacer (ITS) region as a universal DNA barcode marker for Fungi. *Proc. Natl. Acad. Sci. U. S. A.* 109(16)**,** 6241-6246. doi: 10.1073/pnas.1117018109.

Shao, C., Wang, C., Zheng, C., She, Z., Gu, Y., and Lin, Y. (2010). A new anthraquinone derivative from the marine endophytic fungus *Fusarium sp.* (No. b77). *Nat. Prod. Res.* 24(1)**,** 81-85. doi: 10.1080/14786410902836701.

Short, D.P.G., O'Donnell, K., Thrane, U., Nielsen, K.F., Zhang, N., Juba, J.H., et al. (2013). Phylogenetic relationships among members of the *Fusarium solani* species complex in human infections and the descriptions of *F. keratoplasticum sp.* nov. and *F. petroliphilum* stat. nov. *Fungal Genet. Biol.* 53**,** 59-70. doi: 10.1016/j.fgb.2013.01.004.

Singh, M., Kumar, A., Singh, R., and Pandey, K.D. (2017). Endophytic bacteria: a new source of bioactive compounds. *3 Biotech* 7(5)**,** 315. doi: 10.1007/s13205-017-0942-z.

Sun, W., Wu, W., Liu, X., Zaleta-Pinet, D.A., and Clark, B.R. (2019). Bioactive compounds isolated from marine-derived microbes in china: 2009-2018. *Mar. Drugs* 17(6)**,** 26. doi: 10.3390/md17060339.

Tatum, J.H., and Baker, R.A. (1983). Naphthoquinones produced by *Fusarium solani* isolated from citrus. *Phytochemistry* 22(2)**,** 543-547. doi: 10.1016/0031-9422(83)83042-8.

Tatum, J.H., Baker, R.A., and Berry, R.E. (1989). Metabolites of *Fusarium solani*. *Phytochemistry* 28(1)**,** 283-284. doi: 10.1016/0031-9422(89)85062-9.

Thammawong, M., Okadome, H., Shiina, T., Nakagawa, H., Nagashima, H., Nakajima, T., et al. (2011). Distinct distribution of deoxynivalenol, nivalenol, and ergosterol in *Fusarium*-infected japanese soft red winter wheat milling fractions. *Mycopathologia* 172(4)**,** 323-330. doi: 10.1007/s11046-011-9415-9.

Van Gennip, M., Christensen, L.D., Alhede, M., Phipps, R., Jensen, P.Ø., Christophersen, L., et al. (2009). Inactivation of the rhlA gene in *Pseudomonas aeruginosa* prevents rhamnolipid production, disabling the protection against polymorphonuclear leukocytes. *APMIS : acta pathologica, microbiologica, et immunologica Scandinavica* 117(7)**,** 537-546. doi: 10.1111/j.1600-0463.2009.02466.x.

Vásquez-Ocmín, P., Suyyagh-Albouz, S., Cojean, S., Amasifuén, C., Rengifo, E., Cabanillas, B., et al. (2016). Chemical profiling by LC-NMR of plants from *Peruvian Amazonia* with antiparasitic activities. *Planta Med.* 81(S 01)**,** S1-S381. doi: 10.1055/s-0036-1596312.

Vassallo, P., Paoli, C., Rovere, A., Montefalcone, M., Morri, C., and Bianchi, C.N. (2013). The value of the seagrass *Posidonia oceanica*: a natural capital assessment. *Mar. Pollut. Bull.* 75(1-2)**,** 157-167. doi: 10.1016/j.marpolbul.2013.07.044.

Wang, Q.X., Li, S.F., Zhao, F., Dai, H.Q., Bao, L., Ding, R., et al. (2011). Chemical constituents from endophytic fungus *Fusarium oxysporum*. *Fitoterapia* 82(5)**,** 777-781. doi: 10.1016/j.fitote.2011.04.002.

Wang, S., Zhang, L., Liu, L.-Y., Dong, Z.-J., Li, Z.-H., and Liu, J.-K. (2012). Six novel steroids from culture of basidiomycete *Polyporus ellisii*. *Natural Products and Bioprospecting* 2(6)**,** 240-244. doi: 10.1007/s13659-012-0058-4.

Wei, J., and Wu, B. (2020). Chemistry and bioactivities of secondary metabolites from the genus *Fusarium*. *Fitoterapia* 146**,** 104638. doi: 10.1016/j.fitote.2020.104638.

Wiegand, I., Hilpert, K., and Hancock, R.E. (2008). Agar and broth dilution methods to determine the minimal inhibitory concentration (MIC) of antimicrobial substances. *Nat. Protoc.* 3(2)**,** 163-175. doi: 10.1038/nprot.2007.521.

Yamamoto, Y., Kinoshita, Y., Ran Thor, G., Hasumi, M., Kinoshita, K., Koyama, K., et al. (2002). Isofuranonaphthoquinone derivatives from cultures of the lichen *Arthonia cinnabarina* (DC.) Wallr. *Phytochemistry* 60(7)**,** 741-745. doi: 10.1016/s0031-9422(02)00128-0.

Yang, S.-P., Xu, J., and Yue, J.-M. (2003). Sterols from the fungus *Catathelasma imperiale*. *Chin. J. Chem* . 21(10)**,** 1390-1394. doi: 10.1002/cjoc.20030211031.

Yu, S., Li, J., Guo, L., Di, C., Qin, X., and Li, Z. (2019). Integrated liquid chromatography-mass spectrometry and nuclear magnetic resonance spectra for the comprehensive characterization of various components in the Shuxuening injection. *J. Chromatogr.* 1599**,** 125-135. doi: https://doi.org/10.1016/j.chroma.2019.04.008.

Zebiri, I., Gratia, A., Haddad, M., Duca, L., Cabanillas, B., Paloque, L., et al. (2016). Zebiriosides A-P, oleanane saponins isolated by LC-SPE-NMR hyphenation from the roots of *Dendrobangia boliviana*. *Planta Med.* 81(S 01)**,** S1-S381. doi: 10.1055/s-0036-1596462.

Figure 1

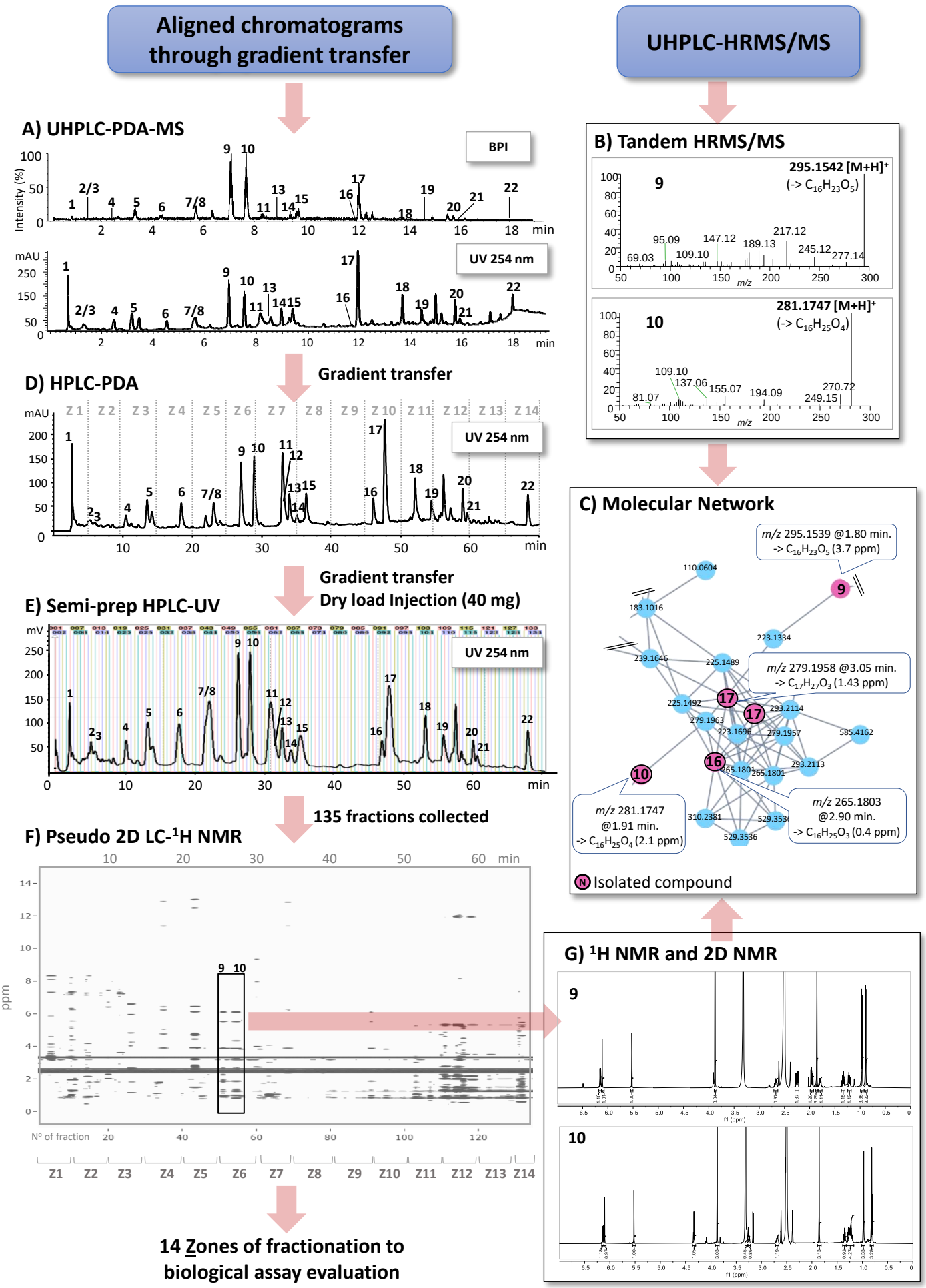
Aligned chromatograms through gradient transfer
UHPLC-HRMS/MS
A) UHPLC-PDA-MS
BPI
UV 254 nm
Intensity (%)
mAU
min
B) Tandem HRMS/MS
295.1542 [M+H]+
(-> C16H23O5)
281.1747 [M+H]+
(-> C16H25O4)
m/z
Gradient transfer
D) HPLC-PDA
Z1 Z2 Z3 Z4 Z5 Z6 Z7 Z8 Z9 Z10 Z11 Z12 Z13 Z14
Gradient transfer
Dry load Injection (40 mg)
E) Semi-prep HPLC-UV
mV
135 fractions collected
C) Molecular Network
m/z 295.1539 @1.80 min.
-> C16H23O5 (3.7 ppm)
m/z 279.1958 @3.05 min.
-> C17H27O3 (1.43 ppm)
m/z 281.1747
@1.91 min.
-> C16H25O4 (2.1 ppm)
m/z 265.1803
@2.90 min.
-> C16H25O3 (0.4 ppm)
Isolated compound
F) Pseudo 2D LC-1H NMR
ppm
N° of fraction
G) 1H NMR and 2D NMR
f1 (ppm)
14 Zones of fractionation to biological assay evaluation

Figure 2

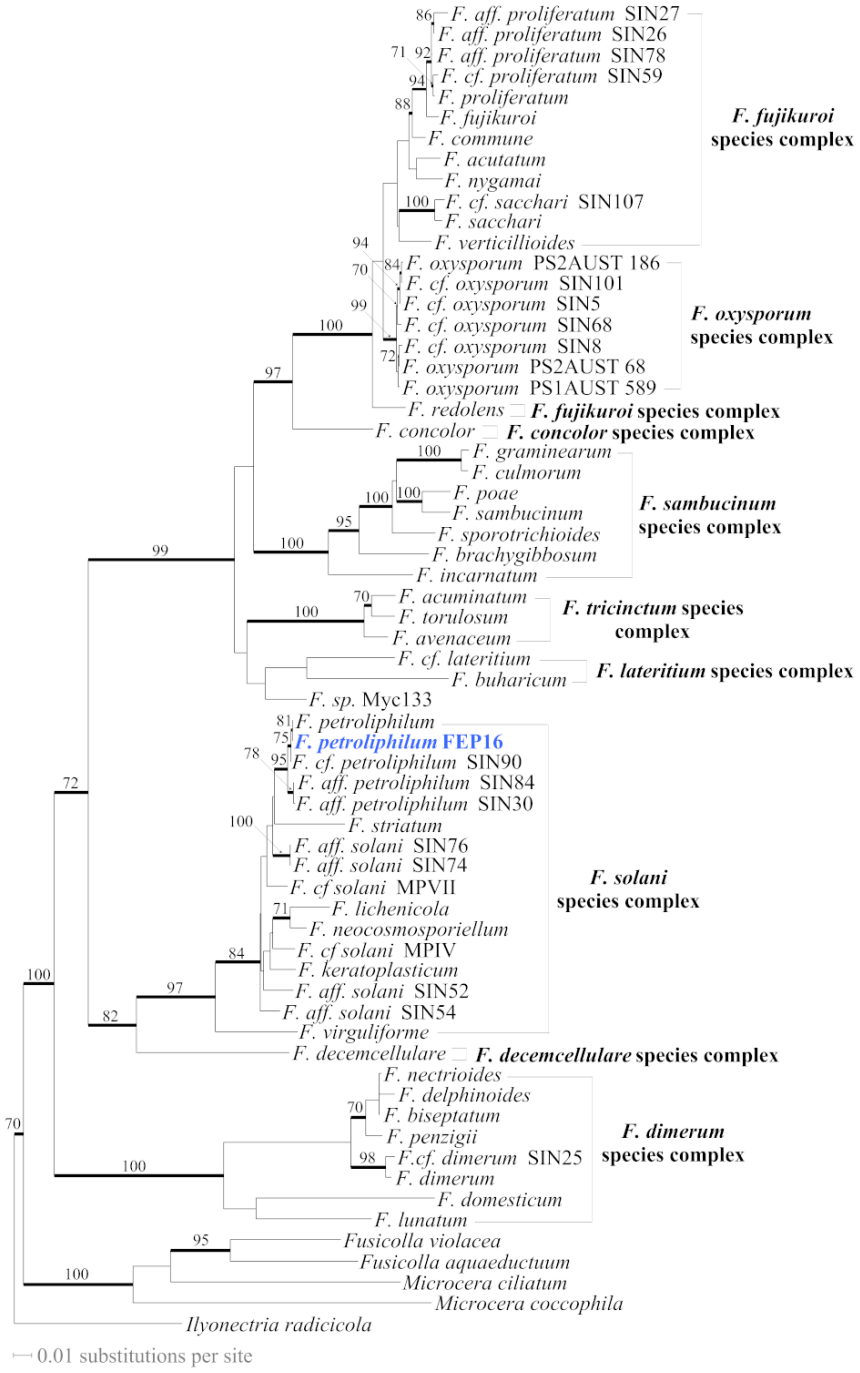
F. aff. proliferatum SIN27
F. aff. proliferatum SIN26
F. aff. proliferatum SIN78
F. cf. proliferatum SIN59
F. proliferatum
F. fujikuroi
F. commune
F. acutatum
F. nygamai
F. cf. sacchari SIN107
F. sacchari
F. verticillioides
F. fujikuroi species complex
F. oxysporum PS2AUST 186
F. cf. oxysporum SIN101
F. cf. oxysporum SIN5
F. cf. oxysporum SIN68
F. cf. oxysporum SIN8
F. oxysporum PS2AUST 68
F. oxysporum PS1AUST 589
F. oxysporum species complex
F. redolens
F. fujikuroi species complex
F. concolor
F. concolor species complex
F. graminearum
F. culmorum
F. poae
F. sambucinum
F. sporotrichioides
F. brachygibbosum
F. sambucinum species complex
F. incarnatum
F. acuminatum
F. torulosum
F. avenaceum
F. tricinctum species complex
F. cf. lateritium
F. buharicum
F. lateritium species complex
F. sp. Myc133
F. petroliphilum
F. petroliphilum FEP16
F. cf. petroliphilum SIN90
F. aff. petroliphilum SIN84
F. aff. petroliphilum SIN30
F. striatum
F. aff. solani SIN76
F. aff. solani SIN74
F. cf solani MPVII
F. lichenicola
F. neocosmosporiellum
F. cf solani MPIV
F. keratoplasticum
F. aff. solani SIN52
F. aff. solani SIN54
F. virguliforme
F. solani species complex
F. decemcellulare
F. decemcellulare species complex
F. nectrioides
F. delphinoides
F. biseptatum
F. penzigii
F.cf. dimerum SIN25
F. dimerum
F. domesticum
F. lunatum
F. dimerum species complex
Fusicolla violacea
Fusicolla aquaeductuum
Microcera ciliatum
Microcera coccophila
Ilyonectria radicicola
0.01 substitutions per site

Figure 3

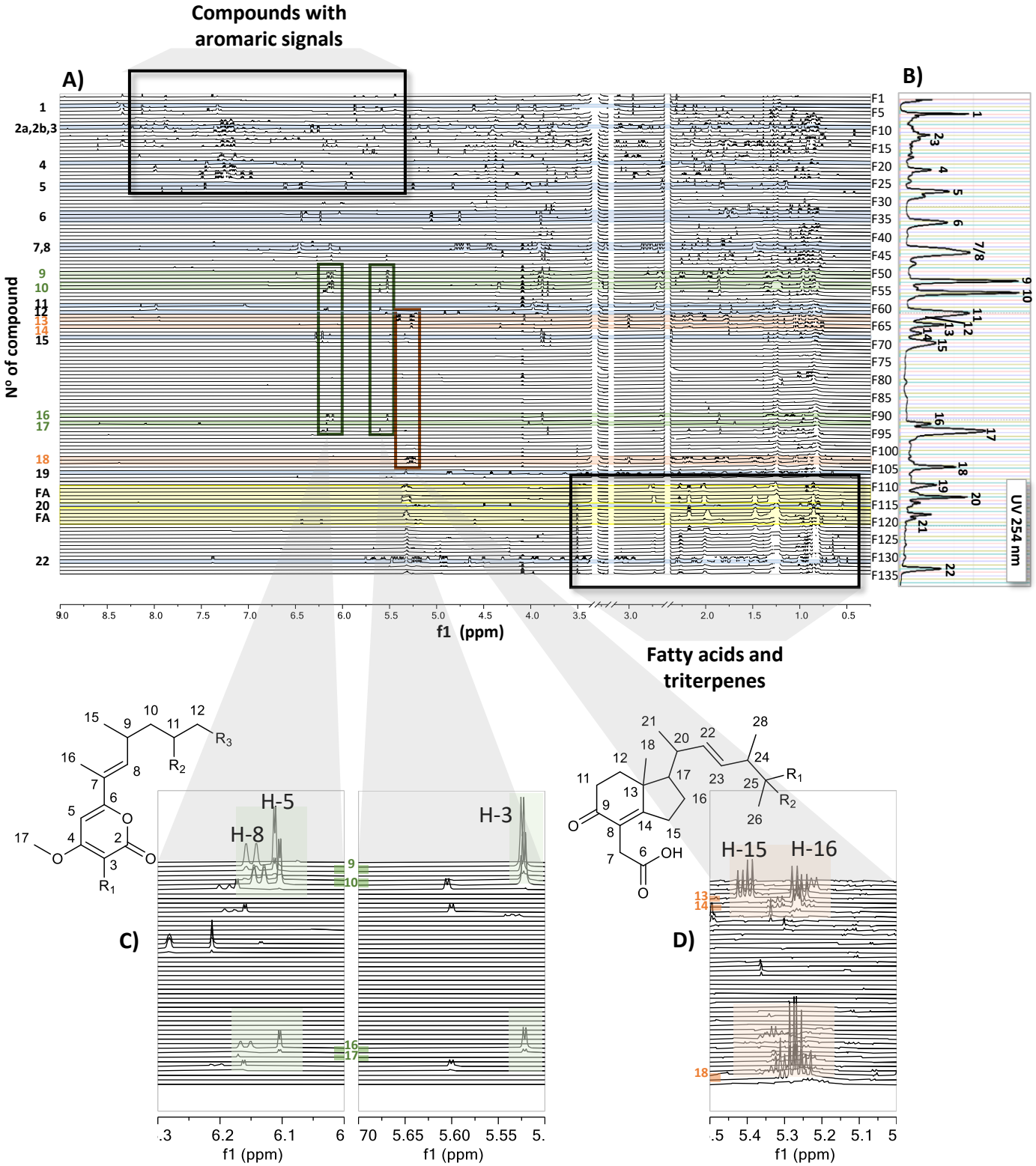
Compounds with aromaric signals
A)
B)
Nº of compound
f1 (ppm)
UV 254 nm
Fatty acids and triterpenes
C)
D)
H-5
H-8
H-3
H-15
H-16
f1 (ppm)

Figure 4

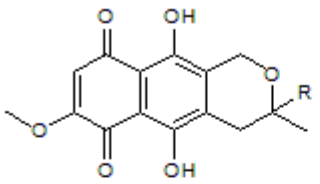

7. R=OH Fusarubin (F43)
8. R=OCH_3 3-O-methylfusarubin (F43)

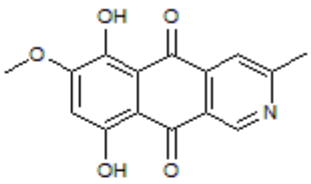

11. Bostrycoidin (F60)

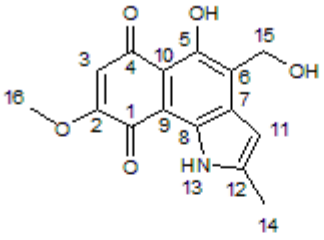

6. (F35)

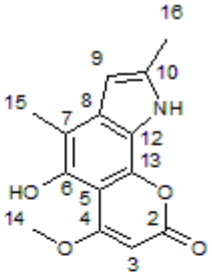

15. (F69)

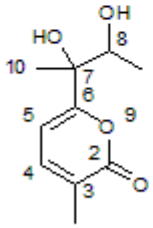

2a/2b. (F10)

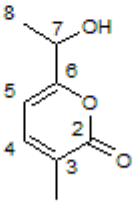

3. (F10)

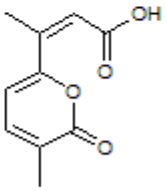

4. Gibepyrone D (F20)

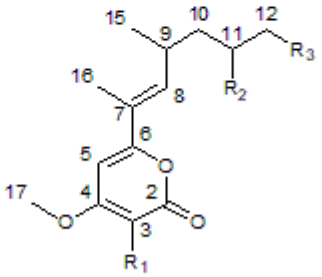

9. R_1 = H R_2=CH_3 R_3=COOH (F51)
10. R_1 = H R_2=CH_2CH_3 R_3=OH (F55)
16. R_1 = H R_2=CH_3 R_3=CH_3 (F91)
17. R_1 = CH_3 R_2=CH_3 R_3=CH_3 (F93)

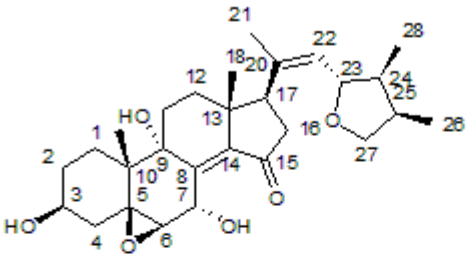

12. (F62)

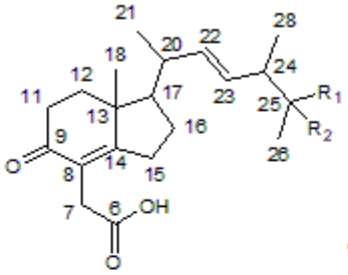

13. R_1 = CH_3 R_2=OH (F64)
14. R_1 = CH_2OH R_2=H (F66)
18. R_1 = CH_3 R_2=H (F103)

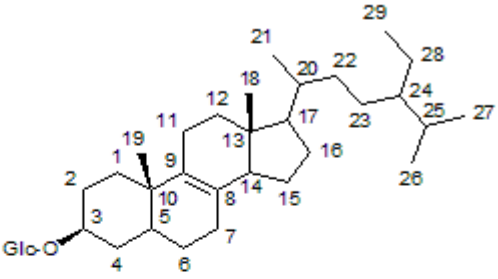

19. (F107)

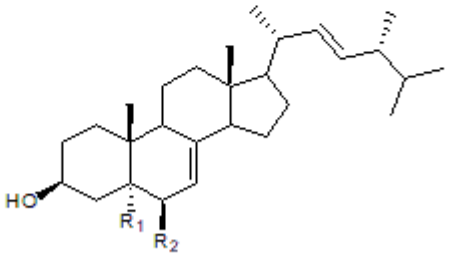

20. R_1=OH R_2=OH Cerevisterol (F116)
21. R_1=OH R_2=H 6-Dehydrocerevisterol (F36_HX)
22. R_1,R_2 C=C Ergosterol (F132)

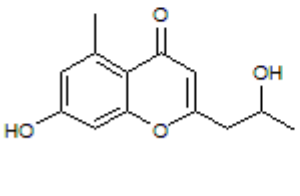

5. Aloesol (F26)

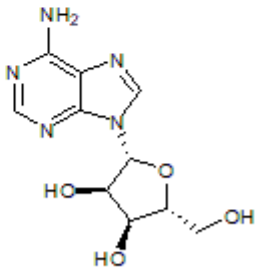

1. Adenosine (F4)

Figure 5

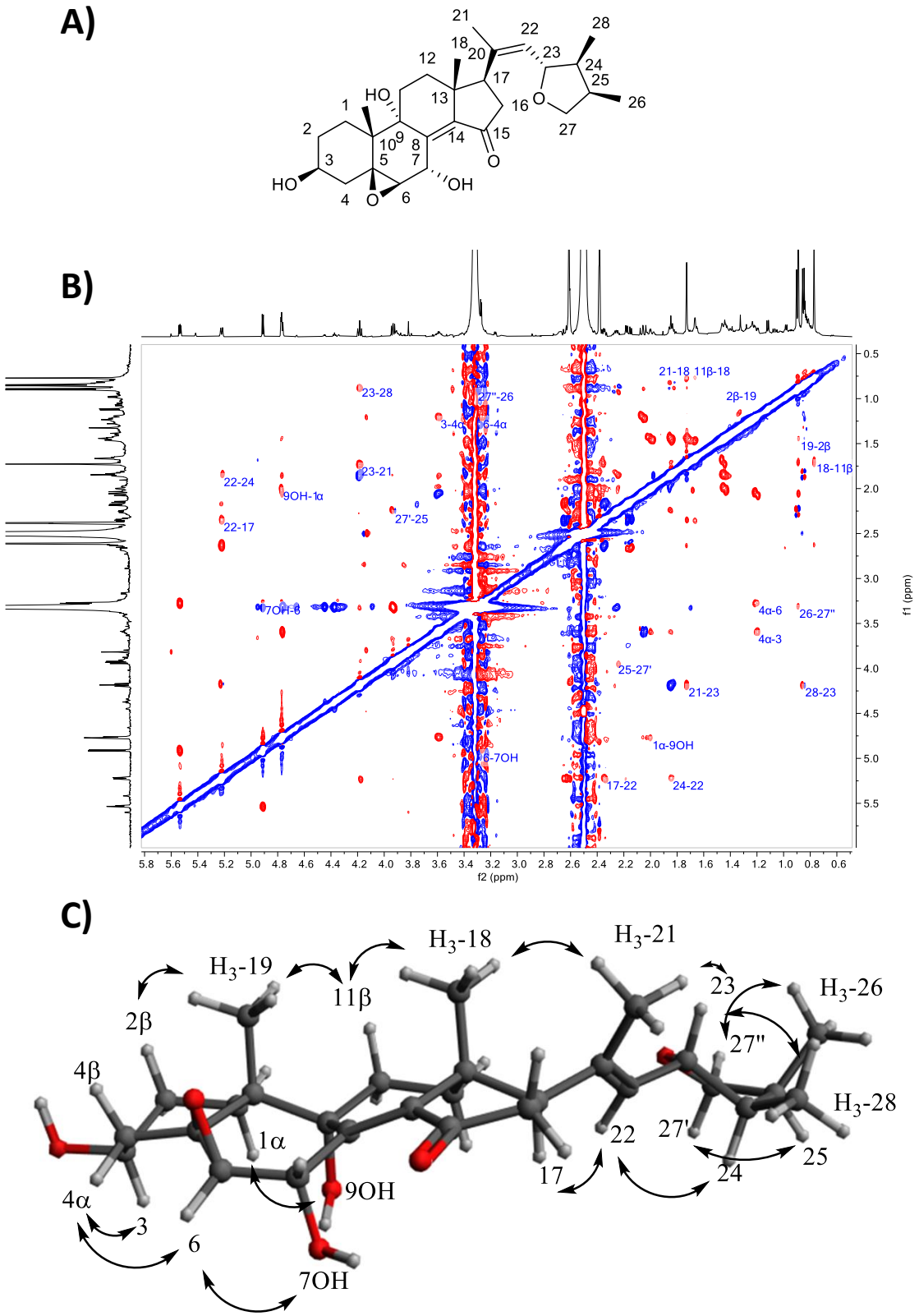
A)
B)
C)
23-28
27''-26
3-4α
6-4α
21-18 11β-18
2β-19
19-2β
18-11β
22-24
9OH-1α
23-21
22-17
27'-25
7OH-6
4α-6
26-27''
4α-3
25-27'
21-23
28-23
1α-9OH
6-7OH
17-22
24-22
f2 (ppm)
f1 (ppm)
H3-19
H3-18
H3-21
2β
11β
23
H3-26
27''
4β
H3-28
1α
22
27'
25
17
24
9OH
4α
3
6
7OH

Figure 6

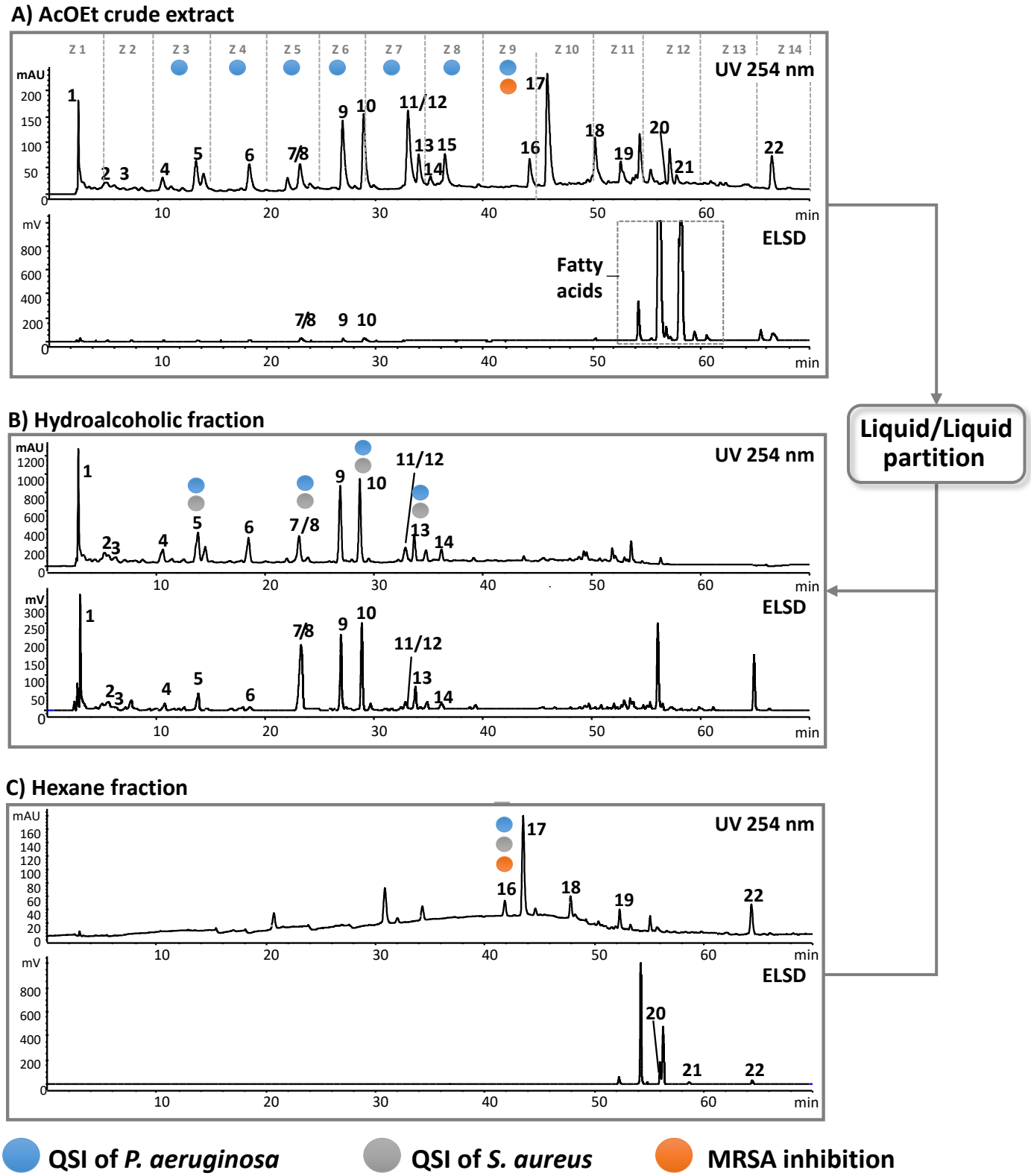
A) AcOEt crude extract
Z 1
Z 2
Z 3
Z 4
Z 5
Z 6
Z 7
Z 8
Z 9
Z 10
Z 11
Z 12
Z 13
Z 14
mAU
UV 254 nm
1
2 3
4
5
6
7/8
9
10
11/12
13
15
14
16
17
18
19
20
21
22
min
mV
ELSD
Fatty acids
B) Hydroalcoholic fraction
Liquid/Liquid partition
C) Hexane fraction
QSI of P. aeruginosa
QSI of S. aureus
MRSA inhibition

Figure 7

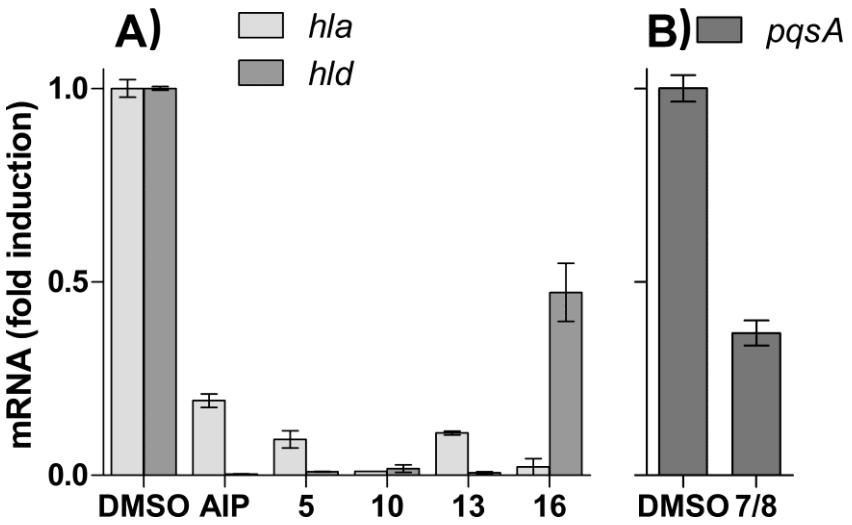
A)
hla
hld
B)
pqsA
mRNA (fold induction)
1.0
0.5
0.0
DMSO
AIP
5
10
13
16
DMSO
7/8